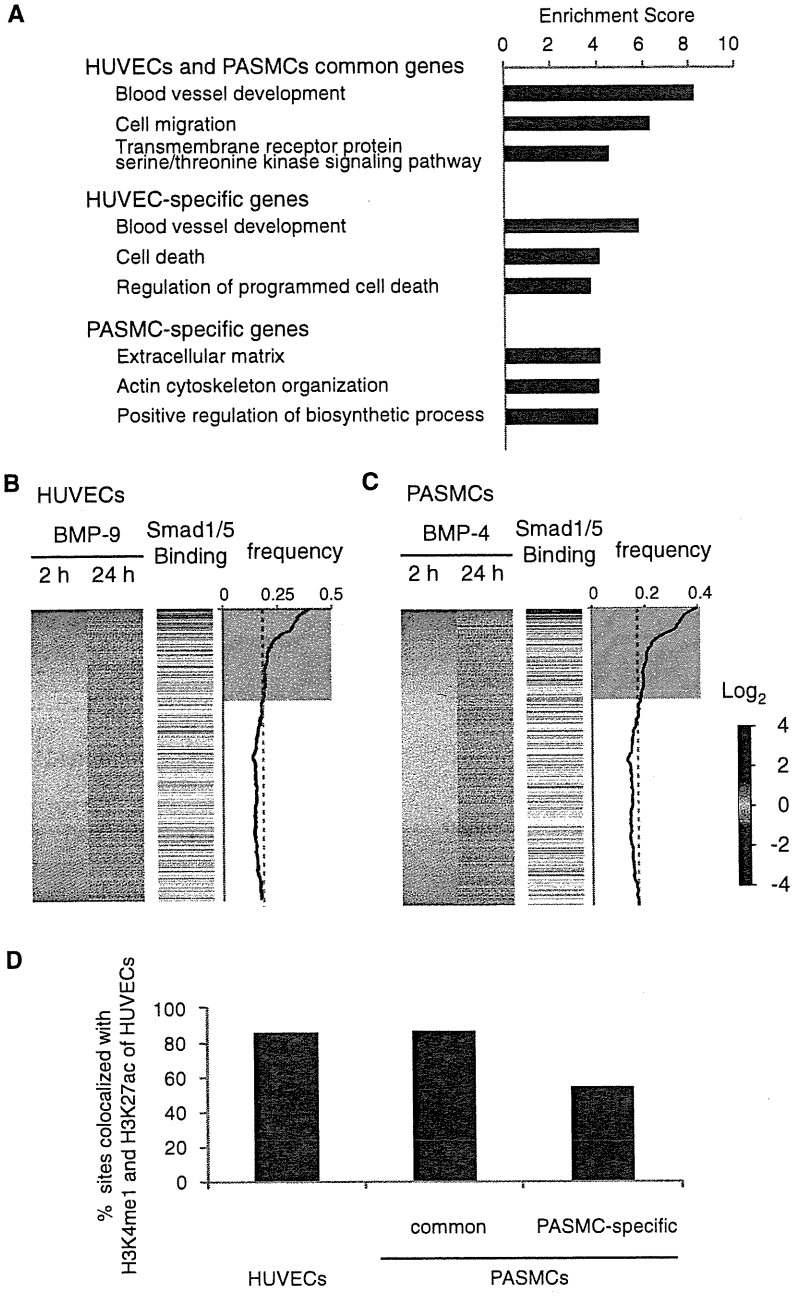

Figure 3. Genome-wide identification of cell type-specific BMP target genes and gene expression profiles. (**A**) GO enrichment analysis was performed to elucidate the biological processes and pathways associated with each gene cluster. The top three annotation clusters are shown in bar plots. The value reflects the Enrichment Score. Group names are based on interpretation of enriched GO annotations. (**B** and **C**) Gene expression profiles of HUVECs with BMP-9 stimulation or PASMCs with BMP-4 are illustrated by heat map. Probes are sorted by fold change relative to time 0 at early phase (2 h after stimulation) (left panel). Increased or decreased mRNA expression is represented by red or blue, respectively. Black horizontal bars represent probes of genes associated with Smad1/5 binding regions (middle panel). Moving average of the frequency of probes with Smad1/5 binding is plotted in a 1000-probe sliding window (right panel). The red-colored areas indicate the probes, whose Smad binding frequency is higher than the expected average. The dashed line indicates the expected average. (**D**) Frequency of the Smad1/5 binding regions co-localized with enhancer regions of HUVECs. The Smad1/5 binding regions in PASMCs are divided into two groups, those shared with HUVECs or PASMC-specific sites.

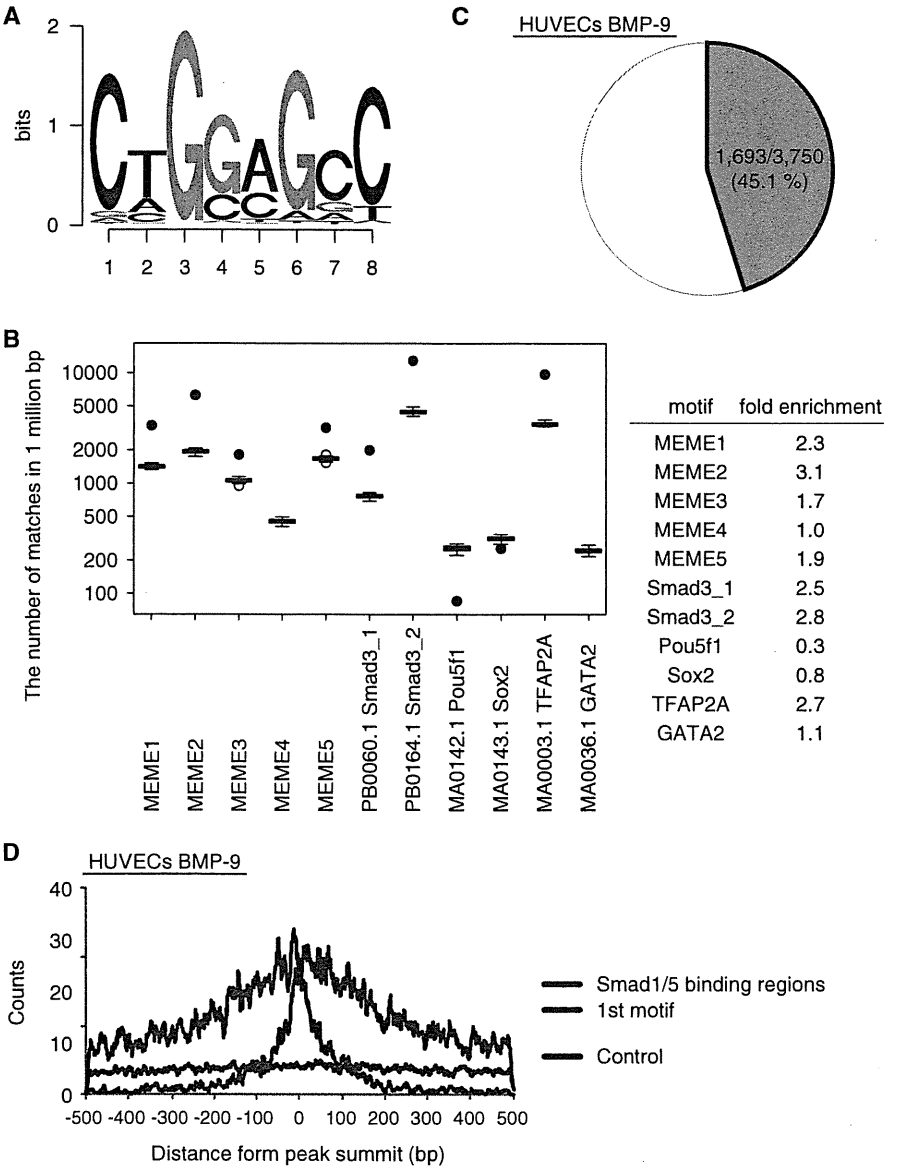

Figure 4. *De novo* prediction of Smad1/5 binding motif. Total 170 peak regions were analyzed for overrepresented motifs using MEME. (**A**) MEME2 is displayed as a sequence logo. (**B**) Enrichment of TFBS in the Smad1/5 binding regions. Fifty sets of non-overlapping matched genomic control sequences were used as background control. Data are given as boxplot. The circles represent outlier values. The black circles indicate the number of matched motifs observed in the Smad1/5 binding regions. (**C**) MEME2 motif occurs in about 45% of all Smad1/5 binding regions in HUVECs stimulated with BMP-9. (**D**) Distribution of MEME2 motif around the peak summits. The number of the MEME2 motif around the peak summits was counted and plotted in a 7 bp sliding window against the distance from the summits (within 500 bp from the summits) (blue). The motifs closest to the summits are located within 100 bp from the peak summit (First motif; green). Five separate matched control regions were randomly chosen by CisGenome and used as a control. The number of the MEME2 motif in those regions was counted and the average was plotted (red).

sequence did not respond to BMP stimulation in PASMCs, whereas mutation to GGCGCC showed a higher responsiveness (Supplementary Figure S5C). Luciferase assays were also performed in HepG2 cells to examine the cell type specificity of the fragments. Similarly, the GGCGCC mutant responded very well compared with wild-type and the T-mutant, while the G-mutant had no enhancer activity in HepG2 (Supplementary Figure S5E).

We next showed the direct binding of recombinant human Smad1 MH1 (rhSmad1 MH1) to the GGAGCC sequence using EMSAs. The amino acid sequence of rhSmad1 MH1 is identical to the corresponding sequence of mouse Smad1 MH1, which was reported to bind to the

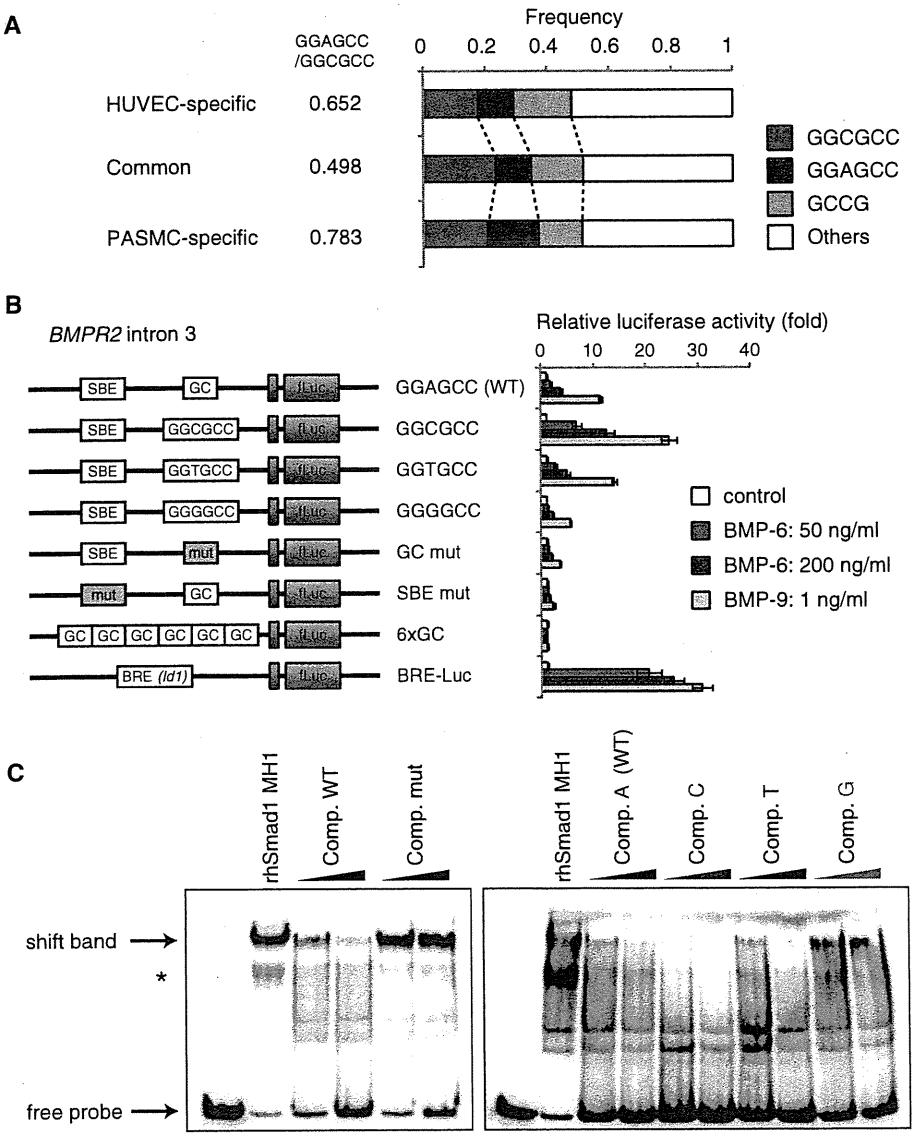

Figure 5. Validation of GGAGCC sequence as a novel BMP responsive element. (**A**) Frequency of GC-SBE sequences in the Smad1/5 binding regions. GGCGCC, GGAGCC and GCCG sequences were enriched in the Smad1/5 binding regions. The ratio of GGAGCC:GGCGCC is indicated. (**B**) pGL4-BMPR2 reporter constructs were introduced into HUVECs using lentiviral vector system, in order to evaluate their enhancer activity. The cells were stimulated with indicated doses of BMP-9 or BMP-6 and then they were harvested and assayed for luciferase activity at 12 h after stimulation. The data are the mean of triplicate values ± SD. (**C**) Recombinant human Smad1 MH1 proteins interacted with GGAGCC sequence. (Left panel) rhSmad1 MH1 binding to the probe was competed with a 50-fold molar excess of the unlabeled wild-type competitor (Comp. WT), but not with the mutant competitor (Comp. mut). (Right panel) To evaluate the importance of 'A' in GGAGCC sequence, single-point mutant competitors were evaluated. An asterisk indicates background band. Full wild-type probe sequence was ACAGCTCT GGAGCC AGATGGCCTGG.

GGCGCC sequence (14). rhSmad1 MH1 was able to bind to the GGAGCC probe and this binding was blocked by wild-type oligonucleotide but not by the mutated one (Figure 5C). The effects of single-point mutation in the GGAGCC sequence were also examined. The GGCGCC sequence competed more efficiently than the GGAGCC sequence, suggesting that this sequence had higher affinity for binding to rhSmad1 MH1 (Figure 5C). Thus, these results showed that the GGAGCC sequence is also a direct binding motif for Smad1/5 and that GC-SBE is a generalized form of the previously reported GC-rich sequences.

Both GC-SBE and SBE are required for full BMP responsiveness

In *Drosophila*, Dpp (Decapentaplegic; *Drosophila* BMP orthologs)-responsive elements are shown to contain a GC-rich Mad binding site and a flanking GTCT Medea

(*Drosophila* Smad4) binding site with a 5 bp spacer sequence (36). Indeed, Smad3 binding motifs were significantly enriched in the Smad1/5 binding regions found in our analysis (Figure 4B). The analysis of the spacer length between GC-SBE and SBE revealed that the 5 bp spacer was also prominent in HUVECs (Figure 6A), suggesting that the 5 bp spacer sequence has some beneficial effect for binding of the Smad complex, containing Smad1/5 and Smad4, in mammalian cells too. On the other hand, expressions of genes associated with the GC-SBE/SBE composite motif with 5 bp spacer were not necessarily regulated by BMP-9 stimulation (Figure 6B).

Next, the roles of SBE sequences, which were located at different distances from GC-SBE, were examined. Evolutionarily conserved SBE/GC-SBE composite motifs with a 28 bp spacer sequence were found in the *BMPR2*

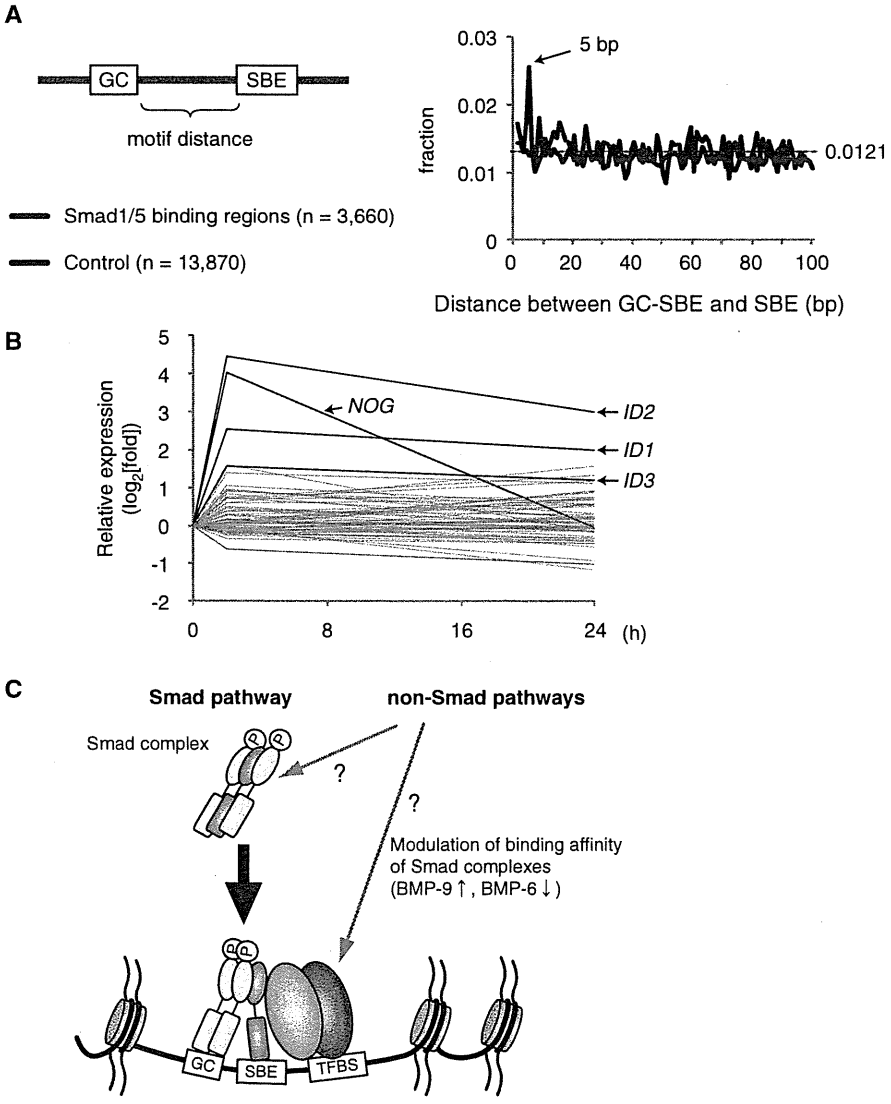

Figure 6. GC-SBE is required, but not sufficient, for full BMP responsiveness. (**A**) The distance between GC-SBE and GTCT-AGAC sequence in Smad1/5 binding regions is calculated and plotted (blue). Total 13 870 GC-SBEs in randomly-adapted control regions were used as a control (red). The dashed line indicates the expected average. (**B**) Graphical summary of expression microarray data of genes with GC-SBE and GTCT-AGAC composite motif with 5 bp spacer. The value of genes with GC-SBE/SBE composite motif with 5 bp spacer is represented as $\log_2$-fold change relative to time 0. Several, but not all of these genes were induced more than 2-fold within 2 h, including the well-known Smad1/5 target genes *ID1*, *ID2*, *ID3* and *NOG* (Noggin) (red). (**C**) Schematic representation of Smad1/5 binding. Smad1/5 binding patterns appear to be predetermined by cell-specific differences in baseline chromatin accessibility patterns. Number and distribution of BR-Smad binding sites over the genome are primarily defined by the intensity of the Smad pathway. Each Smad1/5 binding site has different binding affinity for Smad complexes, which is determined by the affinities of GC-SBEs and SBEs. Non-Smad pathways were reported to affect the BR-Smad signaling through degrading Smad complexes or modulating binding affinity of Smad complexes. GC: GC-SBE, TFBS: transcription factor binding site.

intron 3 and the *JAG1* promoter (Supplementary Figure S5A). These sequences were able to drive luciferase expression in reporter assays in response to BMP stimulation (Figure 5B and Supplementary Figure S5B). Mutations in either GC-SBE or SBE sequence showed significant attenuation of BMP responsiveness (Figure 5B and Supplementary Figure S5B), indicating that the effective distance between GC-SBE and SBE was not restricted to 5 bp. The GC-SBE was not able to respond to BMP stimulation in luciferase reporter assays, even when present in six copies (Figure 5B). These findings clearly showed that both GC-SBE and SBE were required for full BMP responsiveness. Collectively, our results suggest that the binding affinity of Smad complexes to DNA is defined by the affinities of GC-SBEs and SBEs (Figure 6C).

JAG1 is a direct target gene of Smad1/5 in ECs and transactivates Notch signaling in the neighboring cells

EC-specific target genes contained well-known Notch-signal target genes and signaling components, including *HEY1, HEY2, HES1, FOXC1, LFNG, NRARP* and *JAG1* (Figure 7A and Supplementary Table S4). Synergic effects between Notch and BMP signaling on several Notch target genes, such as *HEY1* and *CDH2*, have been reported previously (13,37). However, little is known about direct expression regulation of Notch ligands by BMP signaling in ECs.

Two strong Smad1/5 binding regions were identified in the *JAG1* locus, in the promoter region at −500 bp from the TSS and in the second intron (Figure 7B), which were verified by ChIP–qPCR (Figure 1C). Both regions worked as transcriptional enhancers in HUVECs (Supplementary Figure S5B). Consistent with the results of the reporter assays, BMP-9 was able to induce expression of *JAG1* mRNA (Figure 7C). TNF-α has been shown to induce JAG1 expression in ECs (38). The induction by BMP-9 was equivalent to that of TNF-α and also had some additive effects (Figure 7C). Western blot analysis and immunocytochemistry revealed that the JAG1 protein was also upregulated by BMP-9 stimulation in ECs (Figure 7D and E). This *JAG1* mRNA induction was not affected by CHX, and siRNA against *SMAD4* (siSmad4) attenuated BMP-9-mediated upregulation of *JAG1* (Supplementary Figure S6A and B). These results showed that JAG1 is a direct target gene of BMP-Smad1/5 pathway.

A HeLa reporter cell system was used to verify the function of JAG1 as a Notch ligand. HeLa cells were transfected with the Notch-specific luciferase reporter construct (pGL4-12xCSL-Luc), and thus responsive to Notch activation (26). In the absence of HUVECs, BMP-9 did not induce reporter activity in the transfected HeLa cells (Figure 7F; lanes 1 and 3). In the presence of HUVECs, however, BMP-9 induced strong activation of reporter expression (Figure 7F; lanes 2 and 4), indicating that JAG1 induced by BMP-9 in ECs was able to efficiently transactivate Notch signaling in neighboring cells.

DISCUSSION

In this study, genome-wide maps of Smad1/5 binding regions in human primary cells revealed how BR-Smads recognize and regulate their target genes. Both HUVECs and PASMCs express Smad1, Smad5 and Smad8 (Supplementary Figure S1E). However, redundant functions between Smad1 and Smad5 have been demonstrated *in vivo*, especially in the vasculature (39). *Smad1*$^{+/-}$; *Smad5*$^{+/-}$ double heterozygous mutant mice are embryonic lethal and display defects, which closely resemble those seen in *Smad1*- or *Smad5*-null mice, whereas *Smad1* or *Smad5* single heterozygous mice show no overt phenotype. *Smad8*-null mice additionally lacking one copy of *Smad1* or *Smad5* did not exhibit overt phenotypes, and the tissue disturbances seen in *Smad1*- or *Smad5*-null embryos are not exacerbated in the absence of *Smad8*. These findings suggest that Smad1 and Smad5 possess equivalent biological functions especially in the vasculature, while Smad8 is dispensable.

The mapping data of Smad1/5 showed that ~30% of the binding sites were located in the introns of known genes. Smad1/5 binding peaks of 85.4% overlapped with enhancer regions in HUVECs, where histone modification markers in basal conditions were available. Motif analysis revealed that binding motifs for ETS, AP-1, AP-2 and SP-1 were enriched in Smad1/5 binding regions regardless of the cell types. These motifs were also enriched in the Smad4 binding regions in human keratinocyte HaCaT cells (31). Other motifs occurred only in a small proportion of sequences analyzed. Recently, John and colleagues (40) reported that cell type-specific glucocorticoid receptor binding patterns are comprehensively predetermined by cell-specific differences in baseline chromatin accessibility patterns, with secondary contributions from local sequence features. The similar motif occurrence patterns between HUVECs and PASMCs suggest that the binding regions of BR-Smad are also predetermined in the specific cell types.

Smad1/5 reproducibly bound to some target sites such as *ID1* and *ID3* loci with comparable enrichment after BMP-9 and BMP-6 stimulation, while the total number of Smad1/5 binding sites was dramatically lower in HUVECs treated with BMP-6 compared to those with BMP-9 (3750 versus 880). Increasing the dose of BMP-6 up to 200 ng/ml was not enough to elicit comparable level of enhancer activities as 1 ng/ml BMP-9 (Figures 2C and 5B). This suggests that each binding site has different binding affinity for Smad complex and that BR-Smad signaling through ALK-2 was not enough to occupy full sets of target sites in ECs. This is consistent with the facts that HHT2 is the result of haploinsufficiency of ALK-1 (6), and that ALK-2 signaling is not able to compensate for ALK-1 mutations in HHT patients even though BMP-9 can signal through ALK-2 (1).

In *Drosophila*, Ashe *et al.* (41) have reported that each enhancer element for Mad target genes has a different binding affinity for Smad/Mad. A gene with low-affinity Smad/Mad binding sites is transcribed only in response to high concentrations of Dpp, while a gene with higher affinity sites responds to a low dose of Dpp. Increasing

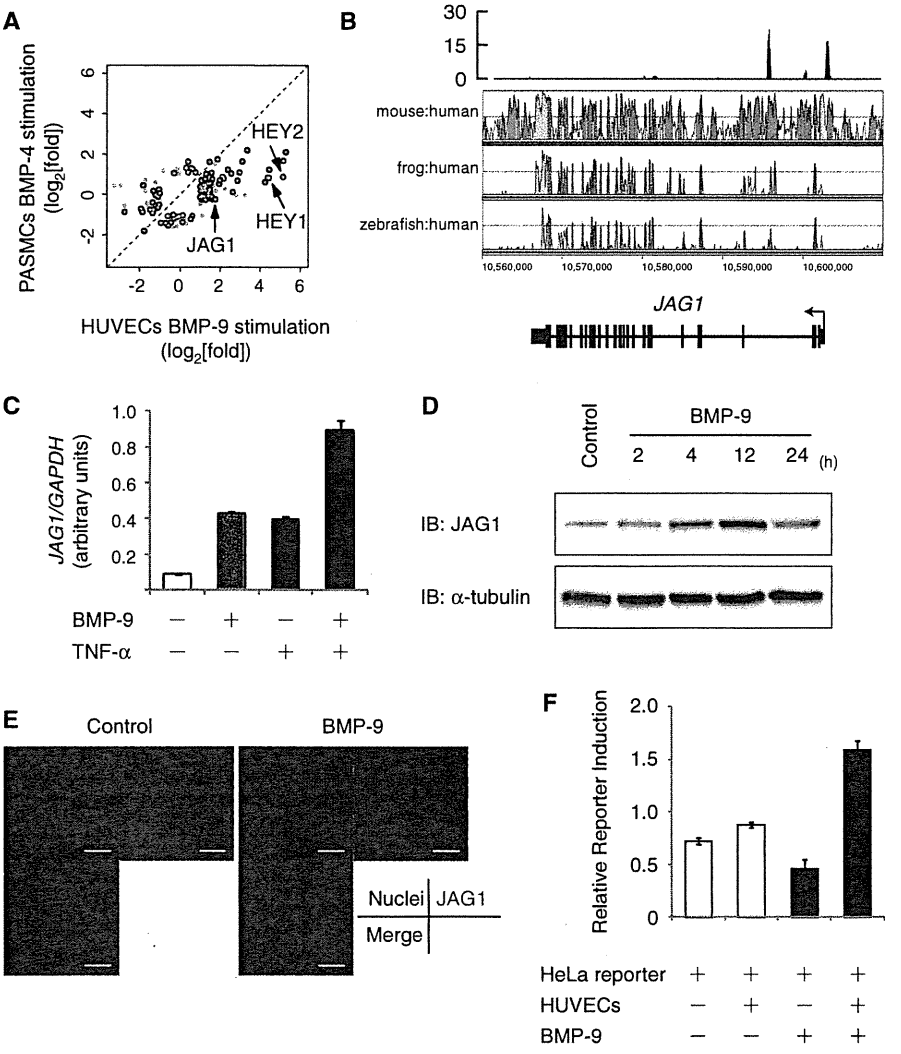

Figure 7. The Notch ligand JAG1 is a direct target gene of Smad1/5 and transactivates Notch signaling in the neighboring cells. (**A**) Scatter plot representation of differentially regulated genes between HUVECs and PASMCs. Probes of genes with more than 2-fold change in expression relative to time 0 are plotted. If the genes are associated with Smad1/5 binding regions of HUVECs (green), PASMCs (red) or both (black), the plots are colored. Signal intensities of HUVECs treated with BMP-9 for 2 h is plotted on the *X*-axis and those of PASMCs treated with BMP-4 for 2 h is plotted on the *Y*-axis. (**B**) Visualization of *JAG1* locus with the result of BMP-9 ChIP-seq. Red peaks represent ChIP regions (top panel). The conservation plots for mouse/human, frog/human and zebrafish/human are derived from VISTA genome browser (middle panel), which represents the sequence conservation between species. (**C**) Induction of *JAG1* after BMP-9 stimulation in HUVECs. HUVECs were starved overnight, stimulated with 1 ng/ml BMP-9 and/or 10 ng/ml TNF-α for 2 h and subjected to qRT–PCR analysis for *JAG1*. Values were normalized to the amount of housekeeping *GAPDH* mRNA. The data are the mean of triplicate values ± SD. (**D**) HUVECs were starved overnight and stimulated with 1 ng/ml BMP-9 for indicated time periods and subjected to immunoblot analysis to determine the JAG1 protein expression level. α-Tubulin was used as a loading control. (**E**) Immunocytochemistry of HUVECs treated with or without 1 ng/ml BMP-9 for 24 h. The cells were immunostained with anti-JAG1 antibody (green). Nuclei were labeled with TOTO-3 (blue). Scale bar, 100 μm. (**F**) Endothelial JAG1 induced by BMP-9 stimulation transactivates Notch signaling in neighboring cells. HeLa cells were transiently transfected with pGL4-12xCSL-luciferase reporter construct and co-cultured with HUVECs. Cells were treated with or without 5 ng/ml BMP-9 for 24 h and subjected to luciferase assay. The data are the mean of triplicate values ± SD.

the affinity of the Smad/Mad binding sites in the enhancer of the *Ance* (also known as *Race*) resulted in a wider expression pattern *in vivo* (42). We revealed that a mutation in our consensus GC-SBE sequences attenuates BMP responsiveness of target genes (Figure 5B and Supplementary Figure S5B). In addition, a mutation of the *HAMP* promoter from GGCGCC to GGTGCC, which was identified in a hemochromatosis patient, impairs the BMP responsiveness *in vivo* and contributes to the severe phenotype (43). These results suggest that the binding affinity for Smad complex is the sum of the affinities of GC-SBEs, SBEs and other DNA binding proteins like

Sox2 and Oct4 in mESCs (16), and that unidentified mutations in the BR-Smad binding regions will be implicated in HHT or PAH.

Collectively, our findings support the notion that BR-Smad binding sites are predetermined in specific cell type and determined by the binding affinity of Smad complex to possible binding sites. It suggests that the strength of the BR-Smad pathway is converted to the number and distribution of BR-Smad binding sites over the genome. It does not necessarily exclude the possibilities that non-Smad pathways play important roles. Non-Smad pathways have been reported to affect the BR-Smad pathway through degrading BR-Smads or modulating binding affinity of Smad complexes [for review, see (44)]. It is possible that they modulate the intensity of BR-Smad pathway and affect the number and distribution of Smad1/5 binding sites in ECs (Figure 6C).

Dysregulation of Notch signaling has been reported to cause AVM [for review, see (45)] that is one of the major pathological features of HHT. JAG1 has been reported to cause differentiation of vascular smooth muscle cell (vSMC) precursor cells and induce vSMC-specific genes *in vitro* through the JAG1-Notch3 signaling pathway (46,47). EC-specific deletion of *Jag1* showed defects in vSMC coverage in mice (38,48). Interestingly, genetic and pharmacological inhibition of ALK-1 signaling showed a severe vascular phenotype including lack of differentiation and recruitment of vSMCs and defects in the maturation phase of angiogenesis (5,49,50). In the clinical settings, thalidomide has been shown to stimulate vessel maturation and have beneficial effects on HHT patients (51). Therefore, our results suggested the important roles of ALK-1-Smad-JAG1 pathway in the pathogenesis of the vascular lesions of the HHT. They also suggest that this pathway will be a novel therapeutic target for treatment of HHT.

ACCESSION NUMBERS

The microarray data from this study have been submitted to NCBI Gene Expression Omnibus (GEO) (http://www.ncbi.nlm.nih.gov/geo) under accession no. GSE27661, and the sequence data from this study have been submitted to the NCBI Sequence Read Archive (http://www.ncbi.nlm.nih.gov/Traces/sra/sra.cgi) under accession no. SRA030442.

SUPPLEMENTARY DATA

Supplementary Data are available at NAR Online.

ACKNOWLEDGEMENTS

The authors are grateful to Drs Aristidis Moustakas and Helen M. Arthur for constructive comments; Kaori Shiina for technical assistance; and members of the Miyazono laboratory for discussion and advice.

FUNDING

KAKENHI grants-in-aid for scientific research on Innovative Area [Integrative Research on Cancer Microenvironment Network (grant number 22112002)]; The Ministry of Education, Culture, Sports, Science and Technology (MEXT), Japan [scientific research (S) grant number 20221009 to H.A.]; Genome Network Project from MEXT (to H.A.); Japan Society for the Promotion of Science (JSPS), the Global Center of Excellence Program (Integrative Life Science Based on the Study of Biosignaling Mechanisms); Swedish Cancer Society (grant number 10 0452). Funding for open access charge: KAKENHI [Integrative Research on Cancer Microenvironment Network (grant number 22112002)].

Conflict of interest statement. None declared.

REFERENCES

1. Miyazono,K., Kamiya,Y. and Morikawa,M. (2010) Bone morphogenetic protein receptors and signal transduction. *J. Biochem.*, **147**, 35–51.
2. Johnson,D.W., Berg,J.N., Baldwin,M.A., Gallione,C.J., Marondel,I., Yoon,S.J., Stenzel,T.T., Speer,M., Pericak-Vance,M.A., Diamond,A. *et al.* (1996) Mutations in the activin receptor-like kinase 1 gene in hereditary haemorrhagic telangiectasia type 2. *Nat. Genet.*, **13**, 189–195.
3. McAllister,K.A., Grogg,K.M., Johnson,D.W., Gallione,C.J., Baldwin,M.A., Jackson,C.E., Helmbold,E.A., Markel,D.S., McKinnon,W.C., Murrell,J. *et al.* (1994) Endoglin, a TGF-beta binding protein of endothelial cells, is the gene for hereditary haemorrhagic telangiectasia type 1. *Nat. Genet.*, **8**, 345–351.
4. Gallione,C.J., Richards,J.A., Letteboer,T.G., Rushlow,D., Prigoda,N.L., Leedom,T.P., Ganguly,A., Castells,A., Ploos van Amstel,J.K., Westermann,C.J. *et al.* (2006) SMAD4 mutations found in unselected HHT patients. *J. Med. Genet.*, **43**, 793–797.
5. Oh,S.P., Seki,T., Goss,K.A., Imamura,T., Yi,Y., Donahoe,P.K., Li,L., Miyazono,K., ten Dijke,P., Kim,S. *et al.* (2000) Activin receptor-like kinase 1 modulates transforming growth factor-beta 1 signaling in the regulation of angiogenesis. *Proc. Natl Acad. Sci. USA*, **97**, 2626–2631.
6. Ricard,N., Bidart,M., Mallet,C., Lesca,G., Giraud,S., Prudent,R., Feige,J.-J. and Bailly,S. (2010) Functional analysis of the BMP9 response of ALK1 mutants from HHT2 patients: a diagnostic tool for novel ACVRL1 mutations. *Blood*, **116**, 1604–1612.
7. Lebrin,F., Goumans,M.-J., Jonker,L., Carvalho,R.L., Valdimarsdottir,G., Thorikay,M., Mummery,C., Arthur,H.M. and ten Dijke,P. (2004) Endoglin promotes endothelial cell proliferation and TGF-beta/ALK1 signal transduction. *EMBO J.*, **23**, 4018–4028.
8. Heldin,C.-H., Miyazono,K. and ten Dijke,P. (1997) TGF-beta signaling from cell membrane to nucleus through SMAD proteins. *Nature*, **390**, 465–471.
9. Yang,X., Long,L., Southwood,M., Rudarakanchana,N., Upton,P.D., Jeffery,T.K., Atkinson,C., Chen,H., Trembath,R.C. and Morrell,N.W. (2005) Dysfunctional Smad signaling contributes to abnormal smooth muscle cell proliferation in familial pulmonary arterial hypertension. *Circ. Res.*, **96**, 1053–1063.
10. International PPH Consortium, Lane,K.B., Machado,R.D., Pauciulo,M.W., Thomson,J.R., Phillips,J.A. 3rd, Loyd,J.E., Nichols,W.C. and Trembath,R.C. (2000) Heterozygous germline mutations in BMPR2, encoding a TGF-beta receptor, cause familial primary pulmonary hypertension. The International PPH Consortium. *Nat. Genet.*, 26, 81–84.

11. Kim,J., Johnson,K., Chen,H.J., Carroll,S. and Laughon,A. (1997) Drosophila Mad binds to DNA and directly mediates activation of vestigial by Decapentaplegic. *Nature*, **388**, 304–308.
12. Korchynskyi,O. and ten Dijke,P. (2002) Identification and functional characterization of distinct critically important bone morphogenetic protein-specific response elements in the Id1 promoter. *J. Biol. Chem.*, **277**, 4883–4891.
13. Itoh,F., Itoh,S., Goumans,M.-J., Valdimarsdottir,G., Iso,T., Dotto,G.P., Hamamori,Y., Kedes,L., Kato,M. and ten Dijke,P. (2004) Synergy and antagonism between Notch and BMP receptor signaling pathways in endothelial cells. *EMBO J.*, **23**, 541–551.
14. BabuRajendran,N., Palasingam,P., Narasimhan,K., Sun,W., Prabhakar,S., Jauch,R. and Kolatkar,P.R. (2010) Structure of Smad1 MH1/DNA complex reveals distinctive rearrangements of BMP and TGF-beta effectors. *Nucleic Acids Res.*, **38**, 3477–3488.
15. Park,P.J. (2009) ChIP-seq: advantages and challenges of a maturing technology. *Nat. Rev.*, **10**, 669–680.
16. Chen,X., Xu,H., Yuan,P., Fang,F., Huss,M., Vega,V.B., Wong,E., Orlov,Y.L., Zhang,W., Jiang,J. *et al.* (2008) Integration of external signaling pathways with the core transcriptional network in embryonic stem cells. *Cell*, **133**, 1106–1117.
17. Fei,T., Xia,K., Li,Z., Zhou,B., Zhu,S., Chen,H., Zhang,J., Chen,Z., Xiao,H., Han,J.-D. *et al.* (2010) Genome-wide mapping of SMAD target genes reveals the role of BMP signaling in embryonic stem cell fate determination. *Genome Res.*, **20**, 36–44.
18. Koinuma,D., Tsutsumi,S., Kamimura,N., Taniguchi,H., Miyazawa,K., Sunamura,M., Imamura,T., Miyazono,K. and Aburatani,H. (2009) Chromatin immunoprecipitation on microarray analysis of Smad2/3 binding sites reveals roles of ETS1 and TFAP2A in transforming growth factor-beta signaling. *Mol. Cell. Biol.*, **29**, 172–186.
19. Ji,H., Jiang,H., Ma,W., Johnson,D.S., Myers,R.M. and Wong,W.H. (2008) An integrated software system for analyzing ChIP-chip and ChIP-seq data. *Nat. Biotechnol.*, **26**, 1293–1300.
20. Bryne,J.C., Valen,E., Tang,M.H., Marstrand,T., Winther,O., da Piedade,I., Krogh,A., Lenhard,B. and Sandelin,A. (2008) JASPAR, the open access database of transcription factor-binding profiles: new content and tools in the 2008 update. *Nucleic Acids Res.*, **36**, D102–D106.
21. Bailey,T.L., Boden,M., Buske,F.A., Frith,M., Grant,C.E., Clementi,L., Ren,J., Li,W.W. and Noble,W.S. (2009) MEME SUITE: tools for motif discovery and searching. *Nucleic Acids Res.*, **37**, W202–W208.
22. Ji,X., Li,W., Song,J., Wei,L. and Liu,X.S. (2006) CEAS: cis-regulatory element annotation system. *Nucleic Acids Res.*, **34**, W551–W554.
23. Nagano,Y., Koinuma,D., Miyazawa,K. and Miyazono,K. (2010) Context-dependent regulation of the expression of c-Ski protein by Arkadia in human cancer cells. *J. Biochem.*, **147**, 545–554.
24. Huang,D.W., Sherman,B.T. and Lempicki,R.A. (2009) Systematic and integrative analysis of large gene lists using DAVID bioinformatics resources. *Nat. Protoc.*, **4**, 44–57.
25. Birney,E., Stamatoyannopoulos,J.A., Dutta,A., Guigo,R., Gingeras,T.R., Margulies,E.H., Weng,Z., Snyder,M., Dermitzakis,E.T., Thurman,R.E. *et al.* (2007) Identification and analysis of functional elements in 1% of the human genome by the ENCODE pilot project. *Nature*, **447**, 799–816.
26. Minoguchi,S., Taniguchi,Y., Kato,H., Okazaki,T., Strobl,L.J., Zimber-Strobl,U., Bornkamm,G.W. and Honjo,T. (1997) RBP-L, a transcription factor related to RBP-Jkappa. *Mol. Cell. Biol.*, **17**, 2679–2687.
27. David,L., Mallet,C., Mazerbourg,S., Feige,J.-J. and Bailly,S. (2007) Identification of BMP9 and BMP10 as functional activators of the orphan activin receptor-like kinase 1 (ALK1) in endothelial cells. *Blood*, **109**, 1953–1961.
28. David,L., Mallet,C., Keramidas,M., Lamande,N., Gasc,J.-M., Dupuis-Girod,S., Plauchu,H., Feige,J.-J. and Bailly,S. (2008) Bone morphogenetic protein-9 is a circulating vascular quiescence factor. *Circ. Res.*, **102**, 914–922.
29. Herrera,B. and Inman,G.J. (2009) A rapid and sensitive bioassay for the simultaneous measurement of multiple bone morphogenetic proteins. Identification and quantification of BMP4, BMP6 and BMP9 in bovine and human serum. *BMC Cell Biol.*, **10**, 20.
30. Valdimarsdottir,G., Goumans,M.-J., Rosendahl,A., Brugman,M., Itoh,S., Lebrin,F., Sideras,P. and ten Dijke,P. (2002) Stimulation of Id1 expression by bone morphogenetic protein is sufficient and necessary for bone morphogenetic protein-induced activation of endothelial cells. *Circulation*, **106**, 2263–2270.
31. Koinuma,D., Tsutsumi,S., Kamimura,N., Imamura,T., Aburatani,H. and Miyazono,K. (2009) Promoter-wide analysis of Smad4 binding sites in human epithelial cells. *Cancer Sci.*, **100**, 2133–2142.
32. Matys,V., Fricke,E., Geffers,R., Gossling,E., Haubrock,M., Hehl,R., Hornischer,K., Karas,D., Kel,A.E., Kel-Margoulis,O.V. *et al.* (2003) TRANSFAC: transcriptional regulation, from patterns to profiles. *Nucleic Acids Res.*, **31**, 374–378.
33. Gupta,S., Stamatoyannopoulos,J.A., Bailey,T.L. and Noble,W.S. (2007) Quantifying similarity between motifs. *Genome Biol.*, **8**, R24.
34. Heintzman,N.D., Hon,G.C., Hawkins,R.D., Kheradpour,P., Stark,A., Harp,L.F., Ye,Z., Lee,L.K., Stuart,R.K., Ching,C.W. *et al.* (2009) Histone modifications at human enhancers reflect global cell-type-specific gene expression. *Nature*, **459**, 108–112.
35. De Val,S. and Black,B.L. (2009) Transcriptional control of endothelial cell development. *Dev. Cell*, **16**, 180–195.
36. Weiss,A., Charbonnier,E., Ellertsdottir,E., Tsirigos,A., Wolf,C., Schuh,R., Pyrowolakis,G. and Affolter,M. (2010) A conserved activation element in BMP signaling during Drosophila development. *Nat. Struct. Mol. Biol.*, **17**, 69–76.
37. Li,F., Lan,Y., Wang,Y., Wang,J., Yang,G., Meng,F., Han,H., Meng,A., Wang,Y. and Yang,X. (2011) Endothelial Smad4 maintains cerebrovascular integrity by activating N-cadherin through cooperation with notch. *Dev. Cell*, **20**, 291–302.
38. Benedito,R., Roca,C., Sorensen,I., Adams,S., Gossler,A., Fruttiger,M. and Adams,R.H. (2009) The notch ligands Dll4 and Jagged1 have opposing effects on angiogenesis. *Cell*, **137**, 1124–1135.
39. Arnold,S.J., Maretto,S., Islam,A., Bikoff,E.K. and Robertson,E.J. (2006) Dose-dependent Smad1, Smad5 and Smad8 signaling in the early mouse embryo. *Dev. Biol.*, **296**, 104–118.
40. John,S., Sabo,P.J., Thurman,R.E., Sung,M.-H., Biddie,S.C., Johnson,T.A., Hager,G.L. and Stamatoyannopoulos,J.A. (2011) Chromatin accessibility pre-determines glucocorticoid receptor binding patterns. *Nat. Genet.*, **43**, 264–268.
41. Ashe,H.L., Mannervik,M. and Levine,M. (2000) Dpp signaling thresholds in the dorsal ectoderm of the Drosophila embryo. *Development*, **127**, 3305–3312.
42. Wharton,S.J., Basu,S.P. and Ashe,H.L. (2004) Smad affinity can direct distinct readouts of the embryonic extracellular Dpp gradient in Drosophila. *Curr. Biol.*, **14**, 1550–1558.
43. Island,M.-L., Jouanolle,A.-M., Mosser,A., Deugnier,Y., David,V., Brissot,P. and Loreal,O. (2009) A new mutation in the hepcidin promoter impairs its BMP response and contributes to a severe phenotype in HFE related hemochromatosis. *Haematologica*, **94**, 720–724.
44. Moustakas,A. and Heldin,C.-H. (2005) Non-Smad TGF-beta signals. *J. Cell Sci.*, **118**, 3573–3584.
45. Gridley,T. (2007) Notch signaling in vascular development and physiology. *Development*, **134**, 2709–2718.
46. Liu,H., Kennard,S. and Lilly,B. (2009) NOTCH3 expression is induced in mural cells through an autoregulatory loop that requires endothelial-expressed JAGGED1. *Circ. Res.*, **104**, 466–475.
47. Doi,H., Iso,T., Sato,H., Yamazaki,M., Matsui,H., Tanaka,T., Manabe,I., Arai,M., Nagai,R. and Kurabayashi,M. (2006) Jagged1-selective notch signaling induces smooth muscle differentiation via a RBP-Jkappa-dependent pathway. *J. Biol. Chem.*, **281**, 28555–28564.
48. High,F.A., Lu,M.M., Pear,W.S., Loomes,K.M., Kaestner,K.H. and Epstein,J.A. (2008) Endothelial expression of

the Notch ligand Jagged1 is required for vascular smooth muscle development. *Proc. Natl Acad. Sci. USA*, **105**, 1955–1959.
49. Niessen,K., Zhang,G., Ridgway,J.B., Chen,H. and Yan,M. (2010) ALK1 signaling regulates early postnatal lymphatic vessel development. *Blood*, **115**, 1654–1661.
50. Hu-Lowe,D.D., Chen,E., Zhang,L., Watson,K.D., Mancuso,P., Lappin,P., Wickman,G., Chen,J.H., Wang,J., Jiang,X. *et al.* (2011) Targeting activin receptor-like kinase 1 inhibits angiogenesis and tumorigenesis through a mechanism of action complementary to anti-VEGF therapies. *Cancer Res.*, **71**, 1362–1373.
51. Lebrin,F., Srun,S., Raymond,K., Martin,S., van den Brink,S., Freitas,C., Breant,C., Mathivet,T., Larrivee,B., Thomas,J.-L. *et al.* (2010) Thalidomide stimulates vessel maturation and reduces epistaxis in individuals with hereditary hemorrhagic telangiectasia. *Nat. Med.*, **16**, 420–428.

nature medicine

RET, ROS1 and ALK fusions in lung cancer

Kengo Takeuchi[1,2], Manabu Soda[3], Yuki Togashi[1,2], Ritsuro Suzuki[4], Seiji Sakata[1], Satoko Hatano[1], Reimi Asaka[1,2], Wakako Hamanaka[2], Hironori Ninomiya[2], Hirofumi Uehara[5], Young Lim Choi[6], Yukitoshi Satoh[5,7], Sakae Okumura[5], Ken Nakagawa[5], Hiroyuki Mano[3,6] & Yuichi Ishikawa[2]

Through an integrated molecular- and histopathology-based screening system, we performed a screening for fusions of anaplastic lymphoma kinase (ALK) and c-ros oncogene 1, receptor tyrosine kinase (ROS1) in 1,529 lung cancers and identified 44 ALK-fusion–positive and 13 ROS1-fusion–positive adenocarcinomas, including for unidentified fusion partners for ROS1. In addition, we discovered previously unidentified kinase fusions that may be promising for molecular-targeted therapy, kinesin family member 5B (KIF5B)-ret proto-oncogene (RET) and coiled-coil domain containing 6 (CCDC6)-RET, in 14 adenocarcinomas. A multivariate analysis of 1,116 adenocarcinomas containing these 71 kinase-fusion–positive adenocarcinomas identified four independent factors that are indicators of poor prognosis: age ≥50 years, male sex, high pathological stage and negative kinase-fusion status.

Echinoderm microtubule associated protein like 4 (EML4)-ALK was the first targetable fusion oncokinase to be identified in non–small cell lung cancer (NSCLC)[1]. This fusion is found in approximately 4–6% of lung adenocarcinomas[2,3]. ROS1 is another receptor tyrosine kinase that forms fusions in NSCLC[4]. Solute carrier family 34 (sodium phosphate), member 2 (SLC34A2)-ROS1 and CD74 molecule, major histocompatibility complex, class II invariant chain (CD74)-ROS1 were identified in 1 out of 41 NSCLC cell lines and 1 out of 150 lung cancer samples, respectively[4]. However, the oncogenic ability of these ROS1 fusion proteins and the incidence of ROS1 fusions in lung cancers are still unclear.

We screened for known and unknown kinase fusions in lung cancers using a histopathology-based system with tissue microarrays of 1,528 surgically removed tissues (**Supplementary Methods** and **Supplementary Appendix**). Immunohistochemistry of antibodies to ALK using the intercalated antibody-enhanced polymer method[2,3,5–7] detected 45 tumors with ALK kinase domain expression (**Supplementary Fig. 1**). In 44 adenocarcinomas, multiplex RT-PCR[2,3] identified 41 *EML4-ALK*–positive and 3 *KIF5B-ALK*–positive adenocarcinomas, including a previously unidentified KIF5B-ALK fusion variant, K17;A20 (**Supplementary Table 1**). Further, we used fluorescence *in situ* hybridization (FISH) for split and fusion assays to confirm the presence of ALK fusions[2,3,8]. The FISH results for the *ALK* split assay, the *EML4-ALK* fusion assay and the *KIF5B-ALK* fusion assay in the 44 adenocarcinomas were all consistent with the presence of the corresponding fusion gene (**Supplementary Figs. 2** and **3**). The remaining tumor that was positive for antibodies to ALK as determined by immunohistochemistry (a large-cell neuroendocrine carcinoma) was negative in the FISH assays and expressed wild-type ALK. ALK fusions existed in 3.0% (44 out of 1,485) of the NSCLCs and 3.9% (44 out of 1,121) of the adenocarcinomas. We included 20 previously reported ALK-fusion–positive and 304 ALK-fusion–negative tumors, all of which were screened with multiplex RT-PCR. Because specimens of these 324 patients were collected consecutively during the period of tissue collection, they served as positive and negative controls, respectively[1–3,8,9]. The immunohistochemistry results using the intercalated antibody-enhanced polymer method were complete matches in the 20 fusion-positive and the 304 fusion-negative tumors.

We used split FISH assays for the screening for *ROS1* gene rearrangement (**Fig. 1**). In 11 of the 13 *ROS1* split FISH-positive tumors (**Fig. 1a**), 5′ rapid amplification of complementary DNA ends (5′ RACE) identified two known and three unknown fusion partners for *ROS1*: *TPM3*, *SDC4*, *SLC34A2*, *CD74* and *EZR* (**Fig. 1b** and **Supplementary Table 1**); RT-PCR confirmed this finding (**Fig. 1c**). In a 5′-RACE–negative tumor (ROS#12) (again, where split FISH is used to detect candidate fusion genes of interest by the presence of rearrangements and RACE is used for the identification of fusion partners), each fusion-specific RT-PCR (using a common reverse primer) amplified the same band, which contained an *LRIG3* sequence. This tumor was proven fusion-positive in RT-PCR specific to *LRIG3-ROS1*, an unidentified fusion. Fusion FISH results confirmed that all 12 cases harbored the corresponding fusion (**Fig. 1a**). All fusion FISH assays for these six ROS1 fusions were negative for the tumor ROS#13 (the frozen material had been consumed), indicating an unknown fusion partner for *ROS1*. *ROS1* split FISH screening failed for nine NSCLCs, including five adenocarcinomas. We identified ROS1 fusions in 0.9% (13 out of 1,476) of the NSCLCs and 1.2% (13 out of 1,116) of the adenocarcinomas.

We performed *KIF5B* split FISH to discover new fusion kinases, as we previously identified KIF5B-ALK fusions in lung cancer[3]. As such, we hypothesized that KIF5B might be rearranged in lung cancer. In 24 *KIF5B* split FISH-positive tumors, 3′ RACE identified an in-frame fusion between *KIF5B* exon 23 and *RET* exon 12

[1]Pathology Project for Molecular Targets, the Cancer Institute, Japanese Foundation for Cancer Research, Tokyo, Japan. [2]Division of Pathology, the Cancer Institute, Japanese Foundation for Cancer Research, Tokyo, Japan. [3]Division of Functional Genomics, Jichi Medical University, Tochigi, Japan. [4]Department of Hematopoietic Stem Cell Transplantation Data Management and Biostatistics, Nagoya University Graduate School of Medicine, Nagoya, Japan. [5]Department of Thoracic Surgical Oncology, Thoracic Center, the Cancer Institute Hospital, Japanese Foundation for Cancer Research, Tokyo, Japan. [6]Department of Medical Genomics, Graduate School of Medicine, University of Tokyo, Tokyo, Japan. [7]Present address: Department of Thoracic Surgery, Kitasato University School of Medicine, Kanagawa, Japan. Correspondence should be addressed to K.T. (kentakeuchi-tky@umin.net).

Received 28 September 2011; accepted 3 January 2012; published online 12 February 2012; doi:10.1038/nm.2658

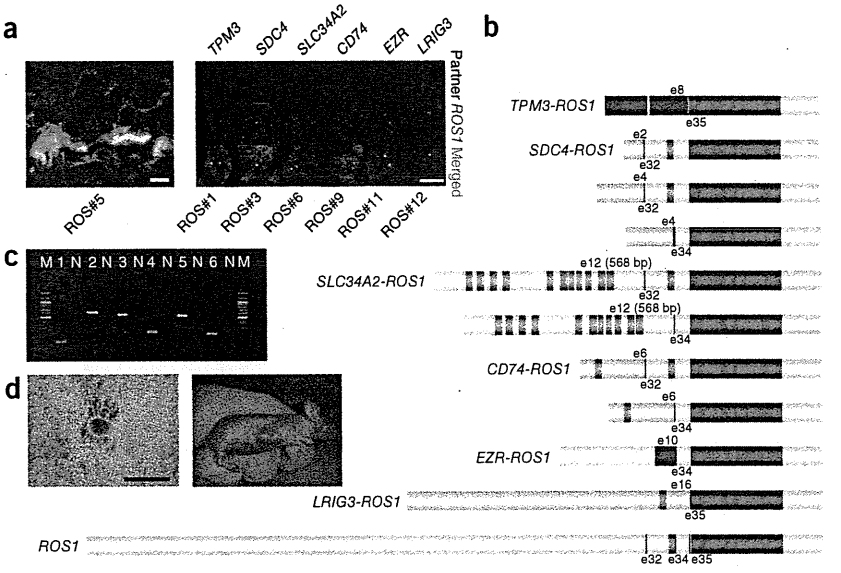

Figure 1 Identification of ROS1 fusions. (**a**) *ROS1* split (left) and fusion (right) FISH assay data (scale bars, 20 μm). In the split assay, multiple tumor cells harbored individual 3′ side signals (green), indicating the presence of a *ROS1* rearrangement. In the fusion assay, a fusion signal (yellow) was observed in the representative tumor cell of each subject, which is consistent with the presence of t(1;6)(q21.2;q22) for *TPM3-ROS1*, t(6;20)(q22;q12) for *SDC4-ROS1*, t(4;6)(q15.2;q22) for *SLC34A2-ROS1*, t(5;6)(q32;q22) for *CD74-ROS1*, inv(6)(q22q25.3) for *EZR-ROS1* or t(6;12)(q22;q14.1) for *LRIG3-ROS1*. (**b**) The break points of ROS1 are exons 32, 34 and 35. All of the break points allow the resulting fusion to harbor the kinase domain of ROS1 (red), and the exon 32 break point allows the resulting fusion to harbor the transmembrane domain of ROS1 (orange). In the fusion partners, dark blue and orange represent coiled-coil and transmembrane domains, respectively. Coiled-coil domains may contribute to homodimelization, but only TPM3 and EZR contained these domains. In contrast to ALK and RET fusions, the role of the fusion partner's coiled-coil domain is unknown in ROS1 fusions. e, exon. (**c**) Results for fusion-specific RT-PCR for tumors ROS#1 (lane 1, TPM3-ROS1, T8;R35, predicted product size of 119 bp), ROS#3 (lane 2, SDC4-ROS1, S2;R32, 596 bp), ROS#6 (lane 3, SLC34A2-ROS1, S13del2046;R32 and S13del2046;R34, 544 bp and 235 bp, respectively), ROS#8 (lane 4, CD74-ROS1, C6;R34, 230 bp), ROS#10 (lane 5, EZR-ROS1, E10;R34, 527 bp), and ROS#12 (lane 6, LRIG3-ROS1, L16;R35, 218 bp). M and N represent the size marker (100-bp ladder) and the non-template control, respectively. (**d**) The transforming potential of the ROS1 fusion. Mouse 3T3 fibroblasts infected with a retrovirus encoding SDC4-ROS1 derived from tumor ROS#4 formed multiple foci (scale bar, 1 mm). All of the four nude mice injected with the corresponding 3T3 cells developed a subcutaneous tumor (right).

(tumor RET#11). *RET* split FISH on the tissue arrays identified 22 fusion-positive tumors in 1,528 lung cancers (**Fig. 2a**), from which a multiplex RT-PCR system that captures all possible *KIF5B-RET* fusions detected 12 fusion-positive tumors: eight tumors with the fusion of *KIF5B* exon 15 and *RET* exon 12 (K15;R12) and one tumor each with the K16;R12, K22;R12, K23;R12 and K24;R11 fusions (**Fig. 2b** and **Supplementary Table 1**). The *KIF5B-RET* fusion FISH results were consistent with the presence of inv(10)(p11.22q11.2) in all 12 of these tumors (**Fig. 2a**).

In a routine histopathological diagnosis, we encountered an adenocarcinoma that showed a mucinous cribriform pattern (**Fig. 2c**) that was previously reported as a histopathological marker for the presence of EML4-ALK (**Supplementary Fig. 4**)[9–11]. Notably, this adenocarcinoma (tumor RET#14) was negative for ALK fusion and was positive for *CCDC6-RET*, as determined by FISH and inverse RT-PCR; the latter fusion gene was first described in thyroid cancer[12]. RT-PCR identified another tumor positive for the *CCDC6-RET* fusion (RET#13) in the remaining 10 tumors. The 14 RET-positive tumors (out of the total 1,528 tumors tested, with one additional tumor (RET#14) found through routine pathology diagnostic service) were also positive in the revised multiplex RT-PCR that captured *EML4-ALK*, *KIF5B-ALK*, *KIF5B-RET* and *CCDC6-RET* simultaneously (**Fig. 2d**). The RET kinase domain expression using real-time RT-PCR was weak or undetectable for the remaining nine tumors determined to be positive in the *RET* split FISH screening. Perhaps the genomic rearrangement occurred downstream of the *RET* break points. *RET* split FISH screening failed in three NSCLCs, including two adenocarcinomas. RET#14 was the index case found in routine pathology diagnostic service but not in the 1,528 cohort. RET fusions existed in 0.9% (13 out of 1,482) of the NSCLCs and 1.2% (13 out of 1,119) of the adenocarcinomas. The 14 RET fusion-positive subjects did not receive vandetanib.

We concluded that the rearrangements described above are somatic without using any matched normal tissues. Our histopathology-based screening method preserves the samples' histological architecture. This allows observers to confirm that internal non-tumor cells, for example, epithelial cells, inflammatory cells or fibroblasts, are negative in a test of interest.

All 71 kinase-fusion–positive (44 ALK, 13 ROS1 and 14 RET fusions) lung cancers were exclusively adenocarcinomas (6% of all adenocarcinomas in the present study), were positive for antibodies to TTF1, which is regarded as a marker for lung adenocarcinoma, as determined by immunohistochemistry (excluding two ALK-positive tumors) and were negative for *EGFR* and *KRAS* mutations. Thirteen of the 44 ALK-positive tumors (30%) were weakly positive for p63 expression (were weakly positive for a squamous cell carcinoma marker, p63) (**Supplementary Table 1**). Thirty-three tumors showed a mucinous cribriform pattern in at least 5% of their area; 22 tumors had this pattern in >25% of their area (**Fig. 2c**, **Supplementary Table 1** and **Supplementary Fig. 4**). The frequency of mucinous cribriform carcinoma was significantly higher in the kinase-fusion–positive group of tumors than in the 77 fusion-negative adenocarcinomas (22 out of 71 compared to 7 out of 77, respectively; $P = 0.00088$). Notably, we observed this pattern preferentially in EML4-ALK–positive tumors (70%, 29 out of 41); all three CD74-ROS1–positive tumors also showed this pattern. Recognizing this pattern in routine pathology diagnoses led to the identification of the CCDC6-RET fusion (tumor RET#14). In organs other than the lung, secretory breast carcinoma, which is characterized by a cribriform pattern with abundant secretory material, harbors the ets variant 6 (ETV6)-neurotrophic tyrosine kinase, receptor, type 3 (NTRK3) fusion (ref. 13). We identified an ALK-fusion–positive renal cell carcinoma that showed a mucinous cribriform pattern[7]. This pattern may be linked to the presence of particular kinase fusions[10], and this possibility warrants further study.

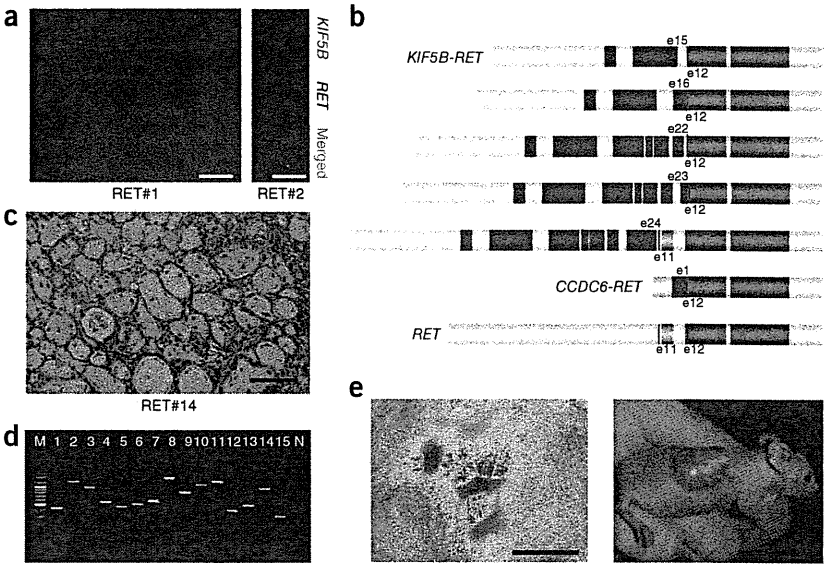

Figure 2 Discovery of RET fusions. (**a**) *RET* split (left) and fusion (right) FISH assay data (scale bars, 20 μm). In the split assay, multiple tumor cells harbored individual 3′ side signals (green), indicating the presence of *RET* rearrangement. In the fusion assay, a fusion signal (yellow) was observed in the representative tumor cell of subject RET#2, which is consistent with the presence of inv(10)(p11.22q11.2). (**b**) The break points of RET are exons 11 and 12. Both of the break points allow the resulting fusion to harbor the kinase domain of RET (red), and the exon 11 break point allows the resulting fusion to harbor the transmembrane domain of RET (orange). In the fusion partners, dark blue represents a coiled-coil domain, which probably contributes to the homodimelization of the fusion. Only the longer isoforms of RET and the RET fusions are shown. (**c**) Subject RET#14 showed the representative histopathology of mucinous cribriform carcinoma (scale bar, 100 μm). (**d**) The results for fusion-specific RT-PCR for subjects ALK#10 (lane 1, EML4-ALK, E13;A20, predicted product size of 432 bp), ALK#16 (lane 2, EML4-ALK, E20;A20, 1185 bp), ALK#26 (lane 3, EML4-ALK, E6;A20, 913 bp), ALK#38 (lane 4, EML4-ALK, E14;ins11del49A20, 546 bp), ALK#39 (lane 5, EML4-ALK, E2;A20, 454 bp), ALK#40 (lane 6, EML4-ALK, E13;ins69A20, 501 bp), ALK#41 (lane 7, EML4-ALK, E14;del14A20, 570 bp), ALK#42 (lane 8, KIF5B-ALK, K17;A20, 1,483 bp), ALK#44 (lane 9, KIF5B-ALK, K24;A20, 814 bp), RET#6 (lane 10, KIF5B-RET, K15;R12, 1,104 bp), RET#9 (lane 11, KIF5B-RET, K16;R12, 1,293 bp), RET#10 (lane 12, KIF5B-RET, K22;R12, 420 bp), RET#11 (lane 13, KIF5B-RET, K23;R12, 525 bp), RET#12 (lane 14, KIF5B-RET, K24;R11, 999 bp) and RET#13 (lane 15, CCDC6-RET, C1;R12, 352 bp). M and N represent the size marker (100-bp ladder) and non-template control, respectively. (**e**) The transforming potential of the KIF5B-RET fusion. Mouse 3T3 fibroblasts infected with a retrovirus encoding K15;R12L derived from tumor RET#7 fomed multiple foci (scale bar, 1 mm). All of the four nude mice injected with the corresponding 3T3 cells developed a subcutaneous tumor (right).

Supplementary Tables 1–4 summarize the clinicopathological features of the subjects. Briefly, young age, low smoking index and small tumor size characterized the kinase-fusion–positive group of subjects (**Supplementary Table 2**). A multivariate analysis of the adenocarcinomas revealed four independent factors that were indicators of poor prognosis: age ≥50 years, male sex, high pathological stage and negative kinase-fusion status (**Supplementary Table 3**). There was no significant difference in overall survival between the kinase-positive and epidermal growth factor receptor (EGFR)-mutant groups (P = 0.32). **Supplementary Table 4** shows the clinicopathological features of the subjects stratified by each fusion.

The transforming ability of CCDC6-RET and all of the ALK fusions, excluding K17;A20, was shown previously[1–3,8,12]. 3T3 cells infected with a virus expressing K17;A20, tropomyosin 3 (TPM3)-ROS1, syndecan 4 (SDC4)-ROS1, SLC34A2-ROS1, CD74-ROS1, ezrin (EZR)-ROS1, leucine-rich repeats and immunoglobulin-like domains 3 (LRIG3) (transcript variant 2)-ROS1 or KIF5B-RET (with both the longer (RET51) and shorter (RET9) RET isoforms) led to multiple transformed foci formation in culture and in subcutaneous tumors in a nude mouse tumorigenicity assay (**Figs. 1d, 2e** and **Supplementary Fig. 5**).

To test whether vandetanib, an inhibitor of vascular endothelial growth factor receptor (VEGFR-2), VEGFR-3, EGFR and RET[14], might be effective for the treatment of RET-fusion–positive tumors, we induced Flag-tagged EML4-ALK (E13;A20) or KIF5B-RET (K15;R12L and K15;R12S) in Ba/F3 cells, which are dependent on interleukin-3 (IL-3) for growth. All transfected cells, including those without any kinase fusion, proliferated in the presence of IL-3, but only cells expressing E13;A20 or K15;R12L grew in the absence of IL-3 (**Supplementary Fig. 6a**). In the absence of IL-3, vandetanib inhibited the proliferation of cells expressing K15;R12L (**Supplementary Fig. 6c**) but not the proliferation of cells expressing E13;A20 (**Supplementary Fig. 6d**). Crizotinib was not effective in inhibiting the proliferation of Ba/F3 cells expressing K15;R12L (**Supplementary Fig. 7**).

In 1985, a 3T3 assay identified *RET* as a rearranged transforming gene[15]. RET fusions have been identified exclusively in papillary thyroid carcinoma and are more frequently observed in radiation-associated thyroid cancers (for example, in survivors of the Chernobyl accident[16], atomic bomb survivors[17] and post-radiation therapy patients[18]). Therefore, a retrospective comparison of RET fusions in individuals with lung cancer with and without a history of radiation exposure warrants further study. If a positive association is found between RET fusion and radiation exposure in these studies, it might be desirable for individuals with internal or therapeutic exposure to irradiation (for example, those individuals involved in the Fukushima accident) to be monitored prospectively for lung cancer as well as thyroid cancer.

In Japan, more than 40% of lung adenocarcinomas in younger individuals harbor EGFR mutations[19]. In this study, 16% (17 out of 107) of younger individuals (≤50 years of age) with adenocarcinoma harbored a kinase fusion. Collectively, as long as molecular target diagnoses are properly performed, >50% of the individuals with lung adenocarcinoma in this generation may benefit from treatment with corresponding kinase inhibitors. Integrated pathology-based screening techniques can also be used for the selection of individuals to receive this treatment[20]. The results of our study will facilitate the development of a molecular classification of lung adenocarcinomas that is closely related to both the pathogenesis and the treatment of disease. This study was approved by the Institutional Review Board of the Cancer Institute Hospital, and all subjects provided informed consent.

METHODS

Methods and any associated references are available in the online version of the paper at http://www.nature.com/naturemedicine/.

Note: Supplementary information is available on the Nature Medicine website.

ACKNOWLEDGMENTS

We thank M. Iwakoshi, K. Shiozawa, T. Kakita, H. Nagano and K. Nomura for their technical assistance and S. Sengoku for providing administrative assistance. This work was supported in part by Grants-in-Aid for Scientific Research from the Ministry of Education, Culture, Sports, Science and Technology of Japan, as well as by grants from the Japan Society for the Promotion of Science; the Ministry of Health, Labor and Welfare of Japan; the Vehicle Racing Commemorative Foundation of Japan; the Princess Takamatsu Cancer Research Fund; and the Uehara Memorial Foundation.

AUTHOR CONTRIBUTIONS

K.T. conceived of and led the entire project, designed the FISH probes, screened samples using FISH and immunohistochemistry, performed histopathological analyses, generated figures and tables and wrote the manuscript. M.S. performed functional analyses and generated the figures. Y.T. performed inverse RT-PCR and RACE experiments and their corresponding analyses. R.S. conducted statistical analyses. S.S. performed FISH and histopathological analyses. S.H. processed and analyzed the tissue microarrays and FISH screening and generated figures. R.A. processed the FISH probe library. W.H. made and analyzed the database and processed tissue microarrays. H.N., H.U., Y.S., S.O. and K.N. collected specimens and clinical information and were involved in planning the project. Y.L.C. conducted functional analyses. H.M. supervised the functional analyses and planned the project. Y.I. performed histopathological analyses and collected specimens. All authors participated in the discussion and interpretation of the data and the results.

COMPETING FINANCIAL INTERESTS

The authors declare no competing financial interests.

Published online at http://www.nature.com/naturemedicine/.
Reprints and permissions information is available online at http://www.nature.com/reprints/index.html.

1. Soda, M. *et al. Nature* **448**, 561–566 (2007).
2. Takeuchi, K. *et al. Clin. Cancer Res.* **14**, 6618–6624 (2008).
3. Takeuchi, K. *et al. Clin. Cancer Res.* **15**, 3143–3149 (2009).
4. Rikova, K. *et al. Cell* **131**, 1190–1203 (2007).
5. Takeuchi, K. *et al. Haematologica* **96**, 464–467 (2011).
6. Takeuchi, K. *et al. Clin. Cancer Res.* **17**, 3341–3348 (2011).
7. Sugawara, E. *et al. Cancer* published online, doi:10.1002/cncr.27391 (17 January 2012).
8. Choi, Y.L. *et al. Cancer Res.* **68**, 4971–4976 (2008).
9. Inamura, K. *et al. J. Thorac. Oncol.* **3**, 13–17 (2008).
10. Takeuchi, K. *Pathol. and Clin. Med.* **28**, 139–144 (2010).
11. Jokoji, R. *et al. J. Clin. Pathol.* **63**, 1066–1070 (2010).
12. Grieco, M. *et al. Cell* **60**, 557–563 (1990).
13. Tognon, C. *et al. Cancer Cell* **2**, 367–376 (2002).
14. Flanigan, J., Deshpande, H. & Gettinger, S. *Biologics* **4**, 237–243 (2010).
15. Takahashi, M., Ritz, J. & Cooper, G.M. *Cell* **42**, 581–588 (1985).
16. Ito, T. *et al. Lancet* **344**, 259 (1994).
17. Hamatani, K. *et al. Cancer Res.* **68**, 7176–7182 (2008).
18. Bounacer, A. *et al. Oncogene* **15**, 1263–1273 (1997).
19. Kosaka, T. *et al. Cancer Res.* **64**, 8919–8923 (2004).
20. Han, B. *et al. Cancer Res.* **68**, 7629–7637 (2008).

Cancer Science
The official journal of the Japanese Cancer Association

Case Report

Small non-mucinous bronchioloalveolar carcinoma with anaplastic lymphoma kinase immunoreactivity: A novel *ALK* fusion gene?

Morio Yamamoto,[1] Kengo Takeuchi,[2] Masaki Shimoji,[1] Tomohiro Maniwa,[1] Mitsuhiro Isaka,[1] Kazuo Nakagawa,[1] Yasuhisa Ohde,[1] Haruhiko Kondo[1] and Takashi Nakajima[3,4]

[1]Department of Thoracic Surgery, Shizuoka Cancer Center, Nagaizumi, Shizuoka; [2]Pathology Project for Molecular Targets, The Cancer Institute, Japanese Foundation for Cancer Research, Koto, Tokyo; [3]Division of Diagnostic Pathology, Shizuoka Cancer Center, Nagaizumi, Shizuoka, Japan

(Received August 30, 2011/Revised October 12, 2011/Accepted October 24, 2011)

Echinoderm microtubule-associated protein-like 4 and anaplastic lymphoma kinase (*EML4–ALK*) and kinesin family member 5B (*KIF5B*)–*ALK* are newly identified transforming fusion oncogenes causing non-small-cell lung cancers. These molecular abnormalities have become detectable using not only molecular biological methods, but also highly sensitive immunohistochemistry. During the immunohistochemical study of ALK expression in adenocarcinoma of the lung, we unexpectedly discovered that a small bronchioloalveolar carcinoma (BAC) showed strong ALK immunoreactivity. However, FISH studies failed to reveal *EML4–ALK* and *KIF5B–ALK* fusion genes in this BAC. These findings suggest the possibility that a novel or unknown *ALK* fusion gene plays a crucial role in BAC development. (*Cancer Sci* 2012; 103: 390–392)

In 2007, a novel transforming fusion gene, echinoderm microtubule-associated protein-like 4 and anaplastic lymphoma kinase (*EML4–ALK*), was isolated from a human lung adenocarcinoma and was clinically detected in 6.7% of human non-small-cell lung cancers (NSCLC).[1] The subsequent extensive studies of *EML4–ALK* in human NSCLC elucidated its clinicopathological characteristics, and established that the adenocarcinoma was a predominant histologic type that frequently developed in younger patients and in never or light smokers.[2–4] In 2009, another novel *ALK* fusion gene, kinesin family member 5B (*KIF5B*)–*ALK*, was identified in lung cancers using a highly sensitive immunohistochemistry-based diagnostic system for ALK-positive lung cancer, named the intercalated antibody-enhanced polymer (iAEP) method.[5]

To confirm the frequency of ALK-positive lung adenocarcinoma in young patients in our hospital, we retrospectively collected 49 adenocarcinoma samples patients who were younger than 50 years, who underwent surgery at Shizuoka Cancer Center Hospital (Shizuoka, Japan) between April 2002 and December 2009, and carried out immunohistochemistry using the iAEP method. Of the 49 adenocarcinomas, only three (6.1%) were immunohistochemically positive for ALK. Of the three adenocarcinomas positive for ALK, one showed an unexpected histology of non-mucinous bronchioloalveolar carcinoma (BAC) with a size <1.0 cm in diameter. Herein, we report a unique ALK-positive BAC case, which failed to demonstrate either *EML4-* or *KIF5B–ALK* fusion genes, but showed *ALK* rearrangement based on a FISH study.

Case Report

Clinical presentation. A 47-year-old Japanese woman, never-smoker, visited our hospital in February 2005 because she had been identified as showing a small abnormal shadow in the right lung by computed tomography. The scan displayed ground-glass opacity with central density in the upper lobe of the lung (Fig. 1), which showed weak ^{18}F-fluorodeoxyglucose accumulation on ^{18}F-fluorodeoxyglucose PET. Six months later, right S2 segmentectomy was carried out for diagnosis and treatment. The postoperative course was uneventful, and the patient achieved disease-free survival of more than 5 years.

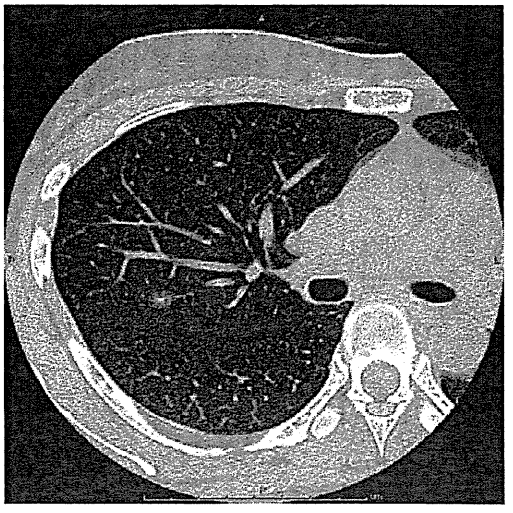

Fig. 1. Chest computed tomography image before surgery. The tumor shows ground-glass attenuation with a solid area in the center.

Tumor histology, immunohistochemistry, and FISH study. The tumor measured 8 × 6 mm, and was located adjacent to the pleura. Collapsed fibrosis with abundant elastic fibers occupied the central area of the tumor (Fig. 2A). The tumor was histologically composed of atypical pneumocytes showing a lepidic growth pattern along the alveolar wall, where many lymphocytic cells infiltrated in some areas (Fig. 2B). The tumor was diagnosed as non-mucinous BAC with collapsed fibrosis (Noguchi's type B). Using routine immunohistochemistry and the iAEP method, tumor cells were positive for thyroid transcription

[4]To whom correspondence should be addressed. E-mail: t.nakajima@scchr.jp

doi: 10.1111/j.1349-7006.2011.02136.x

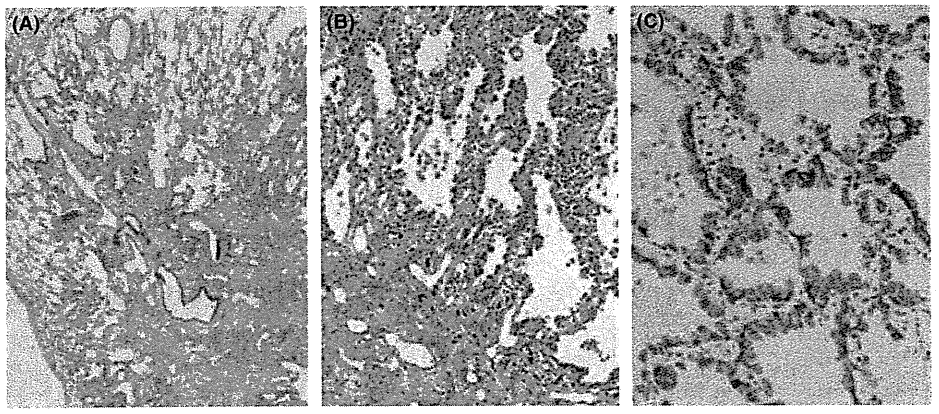

Fig. 2. Histological features of bronchioloalveolar carcinoma (BAC). (A) The tumor was located adjacent to the pleura and contained an area of collapsed fibrosis and an enlarged bronchus in the center (H&E). (B) Tumor cells showed a lepidic growth pattern along the alveolar wall (H&E). (C) Immunohistochemistry for ALK revealed strong expression in the cytoplasm, especially on the basal side of tumor cells.

factor-1 (TTF-1) and ALK, respectively. Immunoreactivity for ALK showed a diffusely fine granular pattern in the cytoplasm of tumor cells and was accentuated in a linear or coarse granular fashion on the basal side of tumor cells (Fig. 2C). In the iAEP method, mouse mAbs against ALK (ALK1 dilution, 1:25; DakoCytomation, Glostrup, Denmark) as a primary antibody, polyclonal rabbit anti-mouse immunoglobulin (Z0259 dilution, 1:400; DakoCytomation), and dextran polymer reagent (K4003; EnVision+ System-HRP labeled polymer; DakoCytomation) were used. The positivity of ALK in this tumor was also confirmed using a commercially available ALK immunohistochemistry kit based on the iAEP method (ALK Detection Kit; Nichirei Bioscience, Tokyo, Japan).

In order to confirm the *ALK* fusion gene in this tumor, the following FISH analyses were carried out: *EML4–ALK* fusion assay (EML4: TexRed, BAC clone RP11-996L7; ALK: FITC, BAC clones RP11-984121, RP11-62B19); *KIF5B–ALK* fusion assay (KIF5B: FITC, BAC clone RP11-460H18; ALK: TexRed, BAC clones RP11-701P18, RP11-62B19); and an *ALK* split assay (LSI ALK Dual Color, Break Apart Rearrangement probe; Abbott, Tokyo, Japan).[5] In both *EML4–ALK* and *KIF5B–ALK* fusion assays, no merged signal was seen in the tumor cell nuclei of the BAC (Fig. 3A,B), indicating that the partner of the gene rearrangement of *ALK* was neither *EML4* nor *KIF5B*. In split FISH analysis for ALK genes, moreover, individual red (3' to ALK) and green (5' to ALK) signals were observed in the tumor nuclei, indicating rearrangement of the ALK locus (Fig. 3C).

Discussion

We present a case of small non-mucinous BAC immunohistochemically positive for ALK. To our knowledge, all ALK-positive NSCLC patients ever reported had invasive or advanced cancers,[1–6] and only three BACs have been confirmed to show no immunoreactivity for ALK.[3] Bronchioloalveolar carcinoma is a pre-invasive lesion and its classification has recently been proposed in the category of adenocarcinoma *in situ*.[7]

Until now, ALK-positive lung adenocarcinoma has revealed characteristic histological features. Namely, *EML4–ALK* adenocarcinoma grows in an acinar pattern with prominent mucin production or a mixed papillary pattern, as well as a solid pattern with signet-ring cells,[3,4,6] in which tumor cells are immunohistochemically positive for TTF-1 and are thought to be derived from cells of the terminal respiratory unit.[8] *KIF5B–ALK* adenocarcinoma reveals a papillary structure different from that of *EML4–ALK* adenocarcinoma.[5] Individual cancer cells contain abundant eosinophilic cytoplasm and more atypical nuclei than those of *EML4–ALK* adenocarcinoma. The histology of ALK-positive BAC is different from those of *EML4–ALK* and *KIF5B–ALK* adenocarcinomas. However, the BAC pattern is histologically observed in *EML4–ALK* adenocarcinoma with mixed subtypes,[4] and it is reasonable to suggest that our ALK-positive BAC is an early lesion of *EML4–ALK* adenocarcinoma. In fact, more than 70% of adenocarcinomas with mixed subtypes contain BAC components, and are likely to have developed from a sequence of BAC through several progression processes.[9]

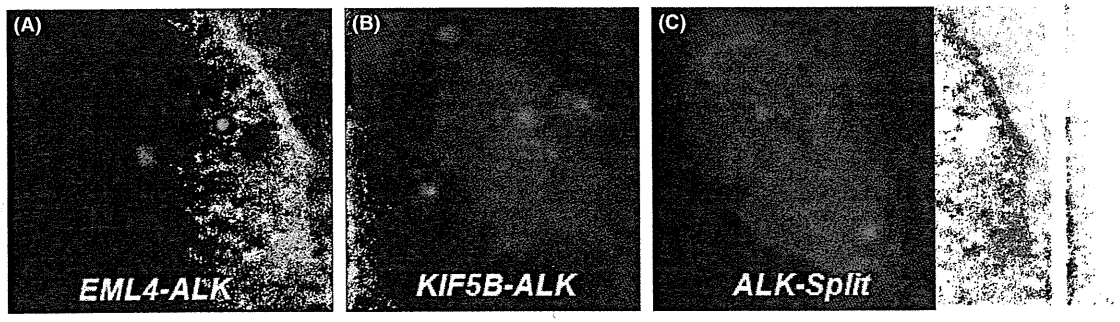

Fig. 3. Fluorescence *in situ* hybridization assay for anaplastic lymphoma kinase (*ALK*) rearrangement. An echinoderm microtubule-associated protein-like 4 (*EML4*)–*ALK* fusion assay (A) and kinesin family member 5B (*KIF5B*)–*ALK* fusion assay (B) showed no merged signals in this case. An *ALK* split assay (C) showed split 5'-side (green) and 3'-side (red) signals, suggesting rearrangement of the *ALK* gene.

As *ALK*-rearranged lung adenocarcinomas invariably express ALK protein, but at much lower levels than in anaplastic large cell lymphoma, highly sensitive immunohistochemistry is necessary to detect ALK expression in lung adenocarcinoma.[5,10] The present BAC case showed strong immunoreactivity for ALK, suggesting *ALK* gene rearrangement. However, a FISH study failed to detect either *EML4–ALK* or *KIF5B–ALK* fusion genes and showed the presence of *ALK* rearrangement in the BAC, which suggests that a novel or unknown *ALK* fusion gene plays a crucial role in BAC development. A *TRK*-fused gene (*TFG*)–*ALK* lung cancer has been reported, but this has not been investigated.[11,12] Moreover, our BAC case developed in a woman who had never smoked, which reminded us of the presence of epidermal growth factor receptor (*EGFR*) gene mutation.[13] In lung cancer development, however, *EGFR* gene mutation is exclusively related to other gene abnormalities, including ALK rearrangement.[2] Further studies are necessary to reach a conclusion regarding this case.

Acknowledgment

The authors thank Mr. Abe (Shizuoka Cancer Center, Nagaizumi, Japan) for his excellent technical assistance.

Disclosure Statement

The authors have no conflicts of interest.

References

1 Soda M, Choi YL, Enomoto M *et al.* Identificaion of the transforming EML4-ALK fusion gene in non-small-cell lung cancer. *Nature* 2007; **448**: 561–6.
2 Inamura K, Takeuchi K, Togashi Y *et al.* EML4-ALK fusion is linked to histological characteristics in a subset of lung cancers. *J Thorac Oncol* 2008; **3**: 13–7.
3 Inamura K, Takeuchi K, Togashi Y *et al.* EML4-ALK lung cancers are characterized by rare other mutations, a TTF-1 cell lineage, an acinar histology, and young onset. *Mod Pathol* 2009; **22**: 508–15.
4 Shaw AR, Yeap BY, Mino-Kenudson M *et al.* Clinical features and outcome of patients with non-small-cell lung cancer who harbor *EML4-ALK*. *J Clin Oncol* 2009; **27**: 4247–53.
5 Takeuchi K, Choi YL, Togashi Y *et al.* KIF5B-ALK, a novel fusiononcokinase identification by an immunohistochemistry-based diagnostic system for ALK-positive lung cancer. *Clin Cancer Res* 2009; **15**: 3143–9.
6 Rodig SJ, Mino-Kenudson M, Dacic S *et al.* Unique clinicopathologic features characterize ALK-rearranged lung adenocarcinoma in the western population. *Clin Cancer Res* 2009; **15**: 5216–23.
7 Travis WD, Brambilla E, Noguchi M *et al.* International association for the study of lung cancer/American Thoracic Society/Europian Respiratory Society International Multidisciplinary Classification of Lung Adenocarcinoma. *J Thorac Oncol* 2011; **6**: 244–85.
8 Tanaka H, Yanagisawa K, Shinjo K *et al.* Lineage-specific dependency of lung adenocarcinomas on the lung development regulator TTF-1. *Cancer Res* 2007; **67**: 6007–11.
9 Gamal G, Sano T, Sakurai S, Kawashima O, Sugano M, Nakajima T. Immunohistopathological re-evaluation of adenocarcinoma of the lung with mixed subtypes using a tissue microarray technique and hierarchical clustering analysis. *Pathol Int* 2007; **57**: 765–74.
10 Mino-Kenudson M, Chirieac LR, Law K, Hornick JL *et al.* A novel, highly sensitive antibody allows for the routine detection of ALK-rearranged lung adenocarcinomas by standard immunohistochemistry. *Clin Cancer Res* 2010; **16**: 1561–71.
11 Rikova K, Guo A, Zeng Q *et al.* Globalsurvey of phosphotyrosine signaling identifies oncogenic kinases in lung cancer. *Cell* 2007; **131**: 1190–203.
12 Shinmura K, Kageyama S, Tao H *et al.* EML4-ALK fusion transcripts, but no NPM-, TPM3-, CLTC-, ATIC-, or TFG-ALK fusion transcripts, in non-small cell lung carcinomas. *Lung Cancer* 2008; **61**: 163–9.
13 Kosaka T, Yatabe Y, Endoh H *et al.* Mutations of the *Epidermal Growth Factor Receptor* gene in lung cancer: biological and clinical implications. *Cancer Res* 2004; **64**: 8919–23.

doi: 10.1111/j.1349-7006.2011.02136.x

Original Article

Identification of Anaplastic Lymphoma Kinase Fusions in Renal Cancer

Large-Scale Immunohistochemical Screening by the Intercalated Antibody-Enhanced Polymer Method

Emiko Sugawara, MD[1,2]; Yuki Togashi, MS[1,3]; Naoto Kuroda, MD[4]; Seiji Sakata, MD, PhD[1]; Satoko Hatano, BS[1,3]; Reimi Asaka, BS[1,3]; Takeshi Yuasa, MD, PhD[5]; Junji Yonese, MD, PhD[5]; Masanobu Kitagawa, MD, PhD[2]; Hiroyuki Mano, MD, PhD[6,7]; Yuichi Ishikawa, MD, PhD[3]; and Kengo Takeuchi, MD, PhD[1,3]

BACKGROUND: Several promising molecular-targeted drugs are used for advanced renal cancers. However, complete remission is rarely achieved, because none of the drugs targets a key molecule that is specific to the cancer, or is associated with "oncogene addiction" (dependence on one or a few oncogenes for cell survival) of renal cancer. Recently, an anaplastic lymphoma kinase (ALK) fusion, vinculin-ALK, has been reported in pediatric renal cell carcinoma (RCC) cases who have a history of sickle cell trait. In this context, ALK inhibitor therapy would constitute a therapeutic advance, as has previously been demonstrated with lung cancer, inflammatory myofibroblastic tumors, and anaplastic large cell lymphomas. **METHODS:** Anti-ALK immunohistochemistry was used to screen 355 tumor tissues, using the intercalated antibody-enhanced polymer (iAEP) method. The cohort consisted of 255 clear cell RCCs, 32 papillary RCCs, 34 chromophobe RCCs, 6 collecting duct carcinomas, 10 unclassified RCCs, 6 sarcomatoid RCCs, and 12 other tumors. **RESULTS:** Two patients (36- and 53-year-old females) were positive for ALK as determined by iAEP immunohistochemistry. Using 5′-rapid amplification of complementary DNA ends, we detected *TPM3-ALK* and *EML4-ALK* in these tumors. The results of this study were confirmed by fluorescence in situ hybridization assays. The 2 ALK-positive RCCs were unclassified (mixed features of papillary, mucinous cribriform, and solid patterns with rhabdoid cells) and papillary subtype. They comprised 2.3% of non-clear cell RCCs (2 of 88) and 3.7% of non-clear cell and nonchromophobe RCCs (2 of 54). **CONCLUSIONS:** The results of this study indicate that ALK fusions also exist in adult RCC cases without uncommon backgrounds. These findings confirm the potential of ALK inhibitor therapy for selected cases of RCC. ***Cancer* 2012;000:000–000.** © *2012 American Cancer Society.*

KEYWORDS: anaplastic lymphoma kinase, molecular-targeted therapy, renal cell carcinoma, immunohistochemistry, intercalated antibody-enhanced polymer.

INTRODUCTION

Renal cancer is one of the major cancers. The incidence and mortality of cases are estimated at 273,518 and 116,368 in the world; 14,963 and 6957 in Japan; and 56,678 and 13,711 in the United States.[1] The 5-year survival rate of patients with localized disease is relatively good: 65% to 93% and 47% to 77% for stages 1 and 2, respectively.[2] For advanced renal cancers (34%-80% and 2%-20% 5-year survival rates in stages 3 and 4, respectively),[2] several molecular-targeted drugs have been recently approved by the US Food and Drug Administration. These drugs, which include sunitinib, sorafenib, temsirolimus, everolimus, bevacizumab, pazopanib, and axitinib, are promising. However, none of them targets a key molecule that is specific to the cancer, or is associated with "oncogene addiction" of renal cancer, namely, the dependence on one or a few oncogenes for maintenance of the malignant phenotype and cell survival.

Anaplastic lymphoma kinase (ALK) fusion is a potential vulnerability, an "Achilles' heel", of many types of human cancer, including lymphoma,[3,4] sarcoma,[5] and carcinoma.[6,7] Experimentally, lung adenocarcinomas developed in EML4-ALK (fusion of ALK with echinoderm microtubule–associated protein like 4) transgenic mice were successfully treated with an ALK inhibitor.[8] The ALK inhibitor crizotinib has recently been used in patients with lung cancer, inflammatory myofibroblastic tumors (IMTs), or anaplastic large cell lymphomas (ALCLs), which harbor various ALK fusions. The compound showed an 81% response rate in ALK-positive lung cancers defined by at least 2 diagnostic methods,[9,10] and a

Corresponding author: Kengo Takeuchi, MD, PhD, Pathology Project for Molecular Targets, The Cancer Institute, Japanese Foundation for Cancer Research, 3-8-31 Ariake, Koto, Tokyo 135-8550, Japan; Fax: (81) 3-3570-0230; kentakeuchi-tky@umin.net

[1]Pathology Project for Molecular Targets, The Cancer Institute, Japanese Foundation for Cancer Research, Tokyo, Japan; [2]Department of Comprehensive Pathology, Graduate School, Tokyo Medical and Dental University, Tokyo, Japan; [3]Division of Pathology, The Cancer Institute, Japanese Foundation for Cancer Research, Tokyo, Japan; [4]Department of Diagnostic Pathology, Kochi Red Cross Hospital, Kochi City, Kochi, Japan; [5]Department of Urology, The Cancer Institute Hospital, Japanese Foundation for Cancer Research, Tokyo, Japan; [6]Division of Functional Genomics, Jichi Medical University, Tochigi, Japan; [7]Department of Medical Genomics, Graduate School of Medicine, University of Tokyo, Tokyo, Japan

We thank Tomoyo Kakita, Keiko Shiozawa, and Motoyoshi Iwakoshi for their technical assistance, and Sayuri Sengoku for providing administrative assistance.

DOI: 10.1002/cncr.27391, **Received:** October 1, 2011; **Revised:** October 31, 2011; **Accepted:** November 10, 2011, **Published online** in Wiley Online Library (wileyonlinelibrary.com)

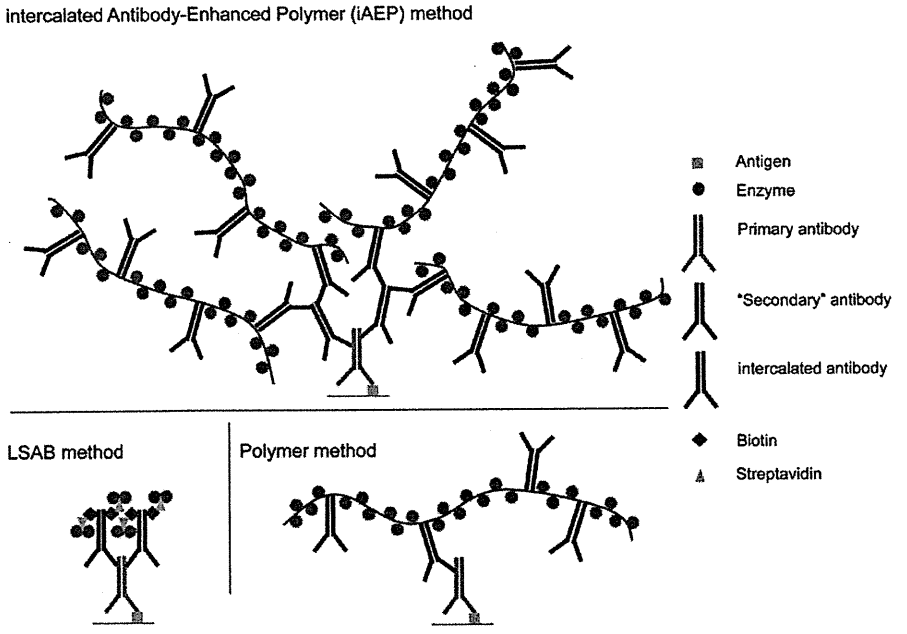

Figure 1. Schematic of intercalated antibody-enhanced polymer (iAEP) method is shown. The labeled streptavidin biotin (LSAB) and polymer methods are common conventional immunohistochemistry methods. In the iAEP method, a step of "intercalated antibody" is added between those of the primary antibody and polymer reagent. Thus, the iAEP method has an additional step compared with the polymer method, but the same number of steps as the LSAB method. There are generally 2 ways to raise the sensitivity of immunohistochemistry. The first is to raise the sensitivity of the antigen-antibody reaction, by increasing the concentration of the primary antibody, using a more sensitive antibody, antigen-retrieval technique, and so forth. The second is to raise the sensitivity of the detection system for the antigen-antibody immune complex. These 2 techniques may appear to generate the same result; however, in principle, they are totally different. The staining results are more likely to differ, especially when the antigen density is very low, such as for EML4-ALK (fusion of echinoderm microtubule-associated protein like 4 with anaplastic lymphoma kinase) or PPFIBP1-ALK (fusion of PTPRF interacting protein binding protein 1 with ALK).[13,24] In such a setting, the latter technique is more advantageous. The staining intensity depends on the density of enzyme in the antigen site. However sensitive a primary antibody is, the antigen-antibody complex cannot exceed the number of antigens. In contrast, it is easy to increase the enzyme density per antigen-antibody complex with use of the latter technique, which includes the iAEP method.

strong response in IMT for several months.[11] Two patients with ALCL who were receiving crizotinib achieved complete remission.[12] These findings indicate that ALK fusion addiction is one of the most promising targets in cancer therapy.

To ensure that such molecular-targeted therapy is effective and less toxic, accurate screening methods to detect ALK fusions are crucial. However, although immunohistochemistry has been a gold standard for the detection of ALK fusions in ALCL and IMT,[13,14] conventional anti-ALK immunohistochemistry is not sensitive enough to detect EML4-ALK, which was first described in lung cancer in 2007.[6,7] To overcome this, we developed a sensitive immunohistochemical tool, the intercalated antibody-enhanced polymer (iAEP) method (Fig. 1).[13] Combined with a conventional anti-ALK mouse monoclonal antibody 5A4, the iAEP method efficiently and consistently detected EML4-ALK in paraffin-embedded sections. In various studies on ALK-positive lung cancer, anti-ALK immunohistochemistry by iAEP or essentially equivalent methods was used to examine surgically resected specimens,[13,15-19] transbronchial lung biopsy specimens,[20] and endobronchial ultrasound-guided transbronchial needle aspiration specimens.[17,21,22] More importantly, some of the patients screened by anti-ALK iAEP immunohistochemical analysis received crizotinib therapy and showed a good response.[16,17,22] Novel ALK fusions, including v6 and v7 of EML4-ALK,[13] kinesin family member 5B (KIF5B)-ALK,[13] sequestosome 1 (SQSTM1)-ALK,[23] and PTPRF interacting protein, binding protein 1 (PPFIBP1)-ALK[24] have been identified using anti-ALK iAEP immunohistochemical analysis. Thus, anti-ALK iAEP immunohistochemistry constitutes a powerful tool for clinical and also research purposes.

The development of anti-ALK antibodies has facilitated the investigation of many types and cases of cancer, including lung cancer.[25-27] Since 1994, ALK-positive tumors have been identified exclusively in lymphoma

(ALCL and ALK-positive large B-cell lymphoma[28]) and sarcoma (IMT,[5] rhabdomyosarcoma,[26] and neuroblastoma[29]). It was not until 2007 that the presence of an ALK fusion was described in lung cancer.[6] This seems to be mainly because EML4-ALK is barely detectable by conventional anti-ALK immunohistochemistry. Considering in reverse, in cases of a tumor that is positive by anti-ALK iAEP immunohistochemistry, but negative by conventional anti-ALK immunohistochemistry, the tumor may have a novel ALK fusion partner, or express wild-type ALK at a modest level. Indeed, in "ALK-negative" IMT cases defined by conventional ALK immunohistochemistry, PPFIBP1-ALK was identified through reassessment for ALK fusions, using anti-ALK iAEP immunohistochemistry.[24] This prompted us to reevaluate other types of solid cancers for ALK fusions. Here, we describe the identification of TPM3-ALK (fusion of tropomyosin 3 and ALK) and EML4-ALK in renal cancer, by anti-ALK iAEP immunohistochemistry.

MATERIALS AND METHODS

Materials

We examined 355 renal tumor tissues from patients who had received surgery in the Cancer Institute Hospital, Japanese Foundation for Cancer Research, Tokyo, between 1994 and 2010. Renal tumors included 255 clear cell renal cell carcinomas (RCCs), 32 papillary RCCs, 34 chromophobe RCCs, 6 collecting duct carcinomas, 10 unclassified RCCs, 6 sarcomatoid RCCs, and 12 other tumors (4 oncocytomas, 3 angiomyolipomas, 1 solitary fibrous tumor, 2 spindle cell sarcomas, 1 desmoplastic sarcoma, and 1 anaplastic carcinoma). Surgically removed tumor specimens were routinely fixed in 20% neutralized formalin and embedded in paraffin for conventional histopathological examination. Immunohistochemical screenings were performed using tissue microarrays. For the 2 cases positive for anti-ALK immunohistochemistry, total RNA was extracted from the corresponding snap-frozen specimen, and purified with the use of an RNeasy Mini kit (Qiagen, Tokyo, Japan). Informed consent was obtained from the patients. The study was approved by the institutional review board of the Japanese Foundation for Cancer Research.

Immunohistochemistry

Formalin-fixed, paraffin-embedded tissue was sliced at a thickness of 4 μm, and the sections were placed on silane-coated slides. For antigen retrieval, the slides were heated for 45 minutes at 102°C in antigen retrieval solution (Nichirei Bioscience, Tokyo). For conventional immunostaining, the slides were incubated at room temperature with primary antibodies: ALK (5A4), vimentin, epithelial membrane antigen (EMA), cytokeratin 7, AE1/AE3, CAM5.2, 34βE12, α-methylacyl-coenzymeA racemase (AMACR), clusters of differentiation 10 (CD10), transcription termination factor 1 (TTF1), renal cell carcinoma marker (RCC Ma), paired box 2 (PAX2), and paired box 8 (PAX8) for 30 minutes. The immune complexes were then detected with polymer reagent (Histofine Simple Stain MAX PO; Nichirei Bioscience, Tokyo, Japan). For the sensitive detection of ALK fusion proteins, the ALK Detection Kit (Nichirei Bioscience), which is based on the iAEP method, was used.

Isolation of ALK Fusions

To obtain complementary DNA (cDNA) fragments corresponding to a novel ALK fusion gene, we used a 5′ rapid amplification of cDNA ends (5′-RACE) method with the SMARTer RACE cDNA Amplification Kit (Clontech, Takara Bio Inc., Shiga, Japan). We followed the manufacturer's instructions, with a minor modification: the ALK2458R primer (5′-GTAGTTGGGGTTGTAGTC GGTCATGATGGT-3′) was used as the gene-specific reverse primer. From the deoxythymidine oligomer–primed cDNA obtained from RNA from case 1, a 385–base pair (bp) cDNA fragment containing the fusion point was specifically amplified with the primers TPM3-705F (5′-AGAGACCCGTGCTGAGTTTGCTG-3′) and ALK3078RR (5′-ATCCAGTTCGTCCTGTTCA GAGC-3′). From case 2, a 454-bp cDNA fragment containing the fusion point was specifically amplified with the primers EML4-72F (5′-GTCAGCTCTTGAGT CACGAGTT-3′) and ALK3078RR. Polymerase chain reaction (PCR) analysis of genomic DNA for TPM3-ALK in case 1 was carried out with a pair of primers flanking the putative fusion point: TPM3-705F (5′-AGA GACCCGTGCTGAGTTTGCTG-3′) and Fusion-RT-AS (5′-TCTTGCCAGCAAAGCAGTAGTTGG-3′). For genomic PCR analysis of EML4-ALK in case 2, we used primers EML4-107F (5′-ATGAAATCACTGTGCTAA AGGCGGCT-3′) and Fusion-RT-AS (5′-TCTTGCCA GCAAAGCAGTAGTTGG-3′).

Fluorescence In Situ Hybridization

Fluorescence in situ hybridization (FISH) analysis of gene fusion was carried out with DNA probes for ALK, TPM3, EML4, and transcription factor E3 (TFE3). Unstained sections (4 μm thick) were subjected to hybridization with an ALK-split probe set (Dako, Tokyo, Japan), TFE3-split probe set (Kreatech, Amsterdam, The Netherlands), or bacterial artificial chromosome (BAC) clone-derived

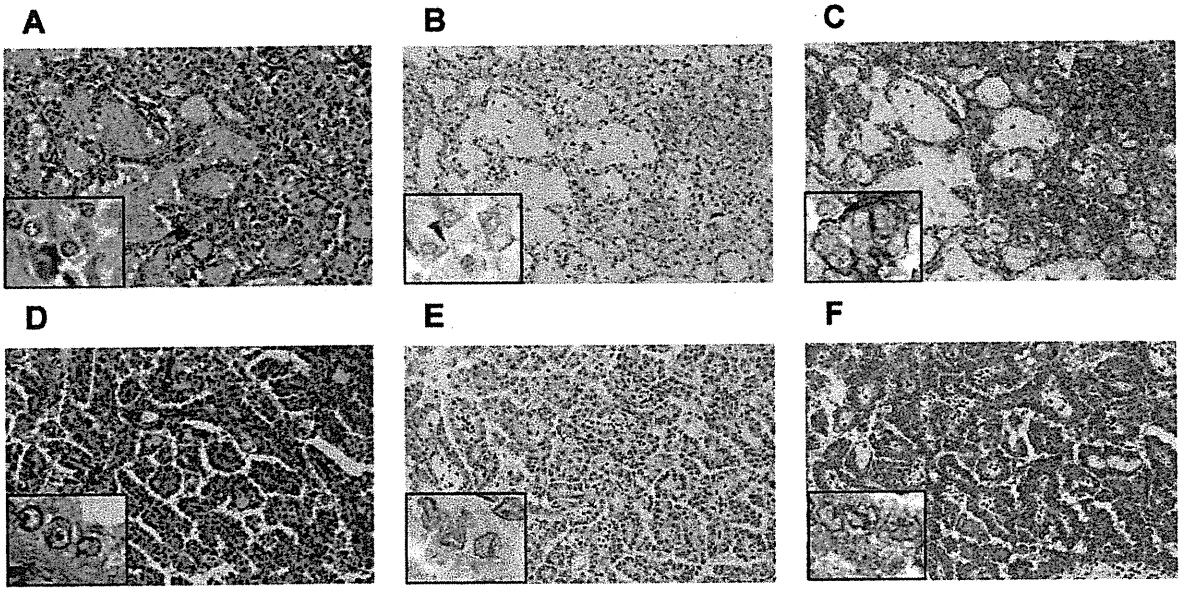

Figure 2. Histopathology of anaplastic lymphoma kinase (ALK)-positive renal cancer. Cuboidal tumor cells showed papillary, tubular, or cribriform growth patterns. The tumor cells had eosinophilic cytoplasm and round to ovoid nuclei. (A) The glandular structures possessed abundant mucin. (D) The tumor comprised a papillary structure of cuboidal or low columnar cells, with eosinophilic cytoplasm and small uniform round to oval nuclei (A,D hematoxylin and eosin stain). The tumor cells were (B) weakly positive and (E) indeterminate for ALK with conventional anti-ALK immunohistochemistry. (C,F) All of the tumor cells were clearly positive for ALK when the iAEP method was used. The staining pattern was diffuse cytoplasmic, with (C) membranous or (F) fine granular accentuation. Figures were taken using the corresponding whole sections (× 10 objective for low power view. × 40 objective for inset). Case 1 (A-C); Case 2 (D-F).

probes for ALK (RP11-984I21, RP11-62B19, RP11-701P18), TPM3 (RP11-809B24), and EML4 (RP11-996L7). Hybridized slides were then stained with 4′,6-diamidino-2-phenylindole and examined using a fluorescence microscope BX51 (Olympus, Tokyo, Japan).

Mutation Analyses for MET

A 1007-bp cDNA fragment containing the MET kinase domain was amplified using the primers MET-3186F (5′-GTCCATTACTGCAAAATACTGTCC-3′) and MET-4193R (5′-CACCTCATCATCAGCGTTATC-3′). The PCR product was sequenced after subcloning.

RESULTS

Identification of ALK Fusions in RCC Samples

Sections of tissue microarray were immunostained for ALK by the iAEP method, resulting in the detection of 2 positive cases (case 1, Fig. 2A-C; case 2, Fig. 2D-F). The positive results were also confirmed using corresponding whole histopathological sections, in which all of the tumor cells stained for ALK as other ALK-positive cancers usually do. We carried out 5′-RACE assays to determine whether these cases expressed ALK fusion or full-length ALK (mutated or unmutated). We isolated a cDNA fragment containing the exon 8 of *TPM3* fused in-frame to the exon 20 of *ALK* (Fig. 3A) in case 1, and the exon 2 of *EML4* fused to the exon 20 of *ALK* in case 2 (Fig. 3B). This EML4-ALK is called variant 5 (E2;A20) in lung cancer.[30] Reverse transcription PCR (RT-PCR) assays designed for the *TPM3-ALK* or E2;A20 successfully amplified cDNAs containing the fusion points (Fig. 3C,D). To confirm the genomic rearrangement, we performed FISH assays (Fig. 4) and genomic PCR (data not shown) for each fusion. All our results were consistent with the presence of t(1;2)(p21;p23)/*TPM3-ALK* in case 1, or inv(2)(p21p23)/E2;A20 in case 2. No other cases were positive for ALK by iAEP immunohistochemistry. All 355 cases were further examined by ALK-split FISH assay. In 12 of the cases, FISH was unsuccessful and not evaluable. In the other cases, the results were identical to those obtained by anti-ALK iAEP immunohistochemistry.

Case Presentation

Case 1

The patient was a 36-year-old woman who had a complaint suggestive of pyelonephritis. Magnetic resonance imaging and computed tomography showed a mass (4.0 cm × 4.0 cm × 3.5 cm) in the left kidney. No metastatic lesions or lymph node enlargements were identified. The patient had no past medical history of malignancy.